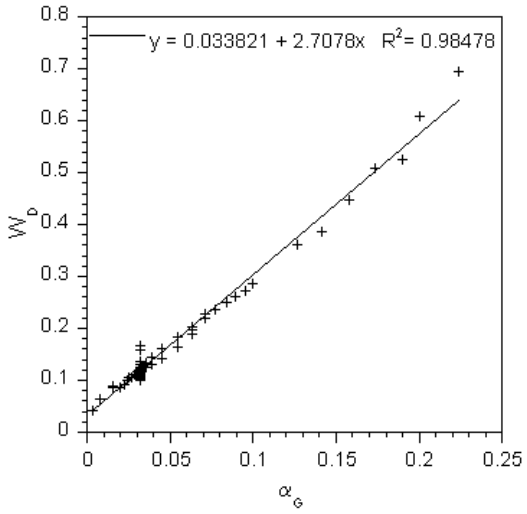

Figure 2.11: Linear relationship of the width of the mixing zone with respect to the geometric mean of the dispersivity coefficients

The resulting expression to determine the vertical width of the mixing zone is

$$F_{WD} \simeq 2.7\,\alpha_G \tag{2.28}$$

To identify the individual role of the longitudinal and transverse dispersivities, several simulations were carried out varying them independently. The concentration distribution of some of these simulations are shown in Figure 2.12. The most extreme cases are not realistic but have been included to exaggerate the individual effect of these parameters.

Figure 2.12 shows that an increase in the longitudinal dispersivity widens the lower part of the mixing zone where the concentration gradient and the velocity vector are parallel. Note that the line of 10% of seawater concentration remains static while the mixing zone broadens downwards and seawards. The freshwater area is not affected, α_L just affects the concentration distribution inside the saltwater wedge. This distribution is consistent with field vertical salinity logs (Figure 2.2A, B and E). They usually display a sharp jump in salinity, but salinity underneath the jump often remains well below seawater concentration. This implies that, at least in those cases,

transverse dispersivity may be much smaller than the $0.1\alpha_L$ value frequently used in practice and adopted here for the base-case.

The effect of increasing transverse dispersivity widens the mixing zone in general. It has a shear effect, bringing the mixing zone backwards at the bottom and inland at the top. As a result, the slope of the isoconcentration lines increases. It must be pointed out that the discharge portion in the seaside boundary becomes wider as the transverse dispersivity increases.

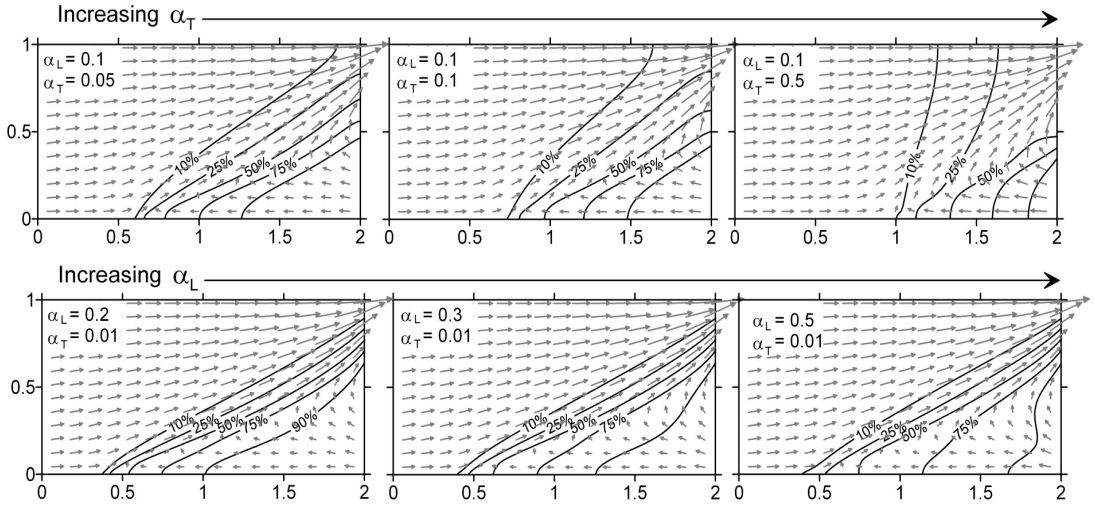

Figure 2.12: Concentration distribution for different simulations showing the effect of increasing independently the longitudinal and the transversal dispersion coefficient

Saltwater mass flux (R_D)

The saltwater mass flux is expected to depend on hydraulic conductivity and freshwater inflow (i.e., the *a* parameter) and the diffusion/ dispersion coefficients (i.e., the Peclet numbers). In fact, if there were no mixing, there would not be any saltwater flux. Still, the question remains about whether it is the transversal or the longitudinal dispersivity what controls the saltwater flux. As for the width of the mixing zone, transverse dispersion is expected to play a more influential role, since most of the mixing occurs orthogonally to the water flux along the mixing zone. *Smith* (2004) has

been one of the few authors that have recently addressed the importance of the quantification of the saltwater mass flux in seawater intrusion studies with velocity dependent dispersion. Although he used a different conceptual model and seaside boundary conditions, his results are relevant to our study. He found an expression to find the ratio between saltwater and freshwater inflow for isotropic and anisotropic case. The expression for the isotropic case fitted accurately his results and others obtained from the literature. His expression for the anisotropic case was not as good, but fairly satisfactory. He found that saltwater flux depends on the geometric average of the hydraulic conductivity, K_G, and the square root of α_T.

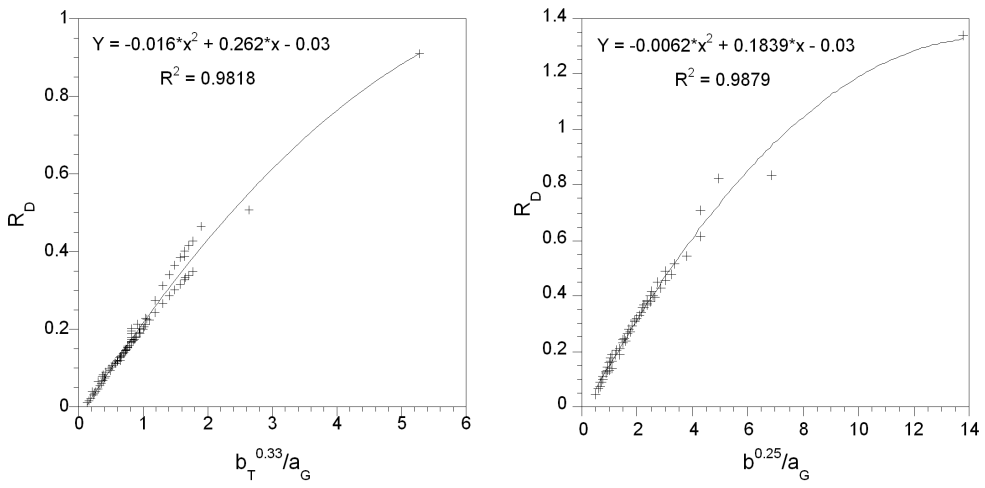

Figure 2.13: Regressions obtained for the dimensionless saltwater flux for the dispersive (left) and diffusive (right) case

We found that the simplest combinations of model parameters that account for a large percentage of the variability on R_D (see Figure 2.13) are:

$$F_{RDS} = \frac{b_T^{\frac{1}{3}}}{a_G} \qquad \text{for the dispersive problem} \tag{2.29}$$

$$F_{RDF} = \frac{b^{\frac{1}{4}}}{a_G} \qquad \text{for the diffusive problem} \tag{2.30}$$

where $b_T = \alpha_T/d$ is the lateral dispersion Peclet number and $a_G = q_b/\epsilon K_G$ with $K_G = \sqrt{K_x K_y}$. The resulting relationships between R_D and F_R are shown in Figure 2.13. Notice that the relationship is nearly linear for $F_RDS < 2$ and $F_RDF < 4$. In such case, the volumetric salt flux becomes

$$q_s = q_b R_D \simeq 0.26\epsilon(\frac{\alpha_T}{d})^{\frac{1}{3}} K_G \tag{2.31}$$

$$q_s = q_b R_D \simeq 0.16\epsilon(\frac{D_m}{q_b d})^{\frac{1}{4}} K_G \tag{2.32}$$

That is, seawater flux is essentially proportional to K_G and $\alpha_T^{\frac{1}{3}}$ (and independent of q_b!).

2.5 Discussion and conclusions

The traditional Henry problem has played a significant historical role in our understanding of seawater intrusion, but displays severe limitations both as a paradigm and as a benchmark test for density dependent flow codes. We state that these drawbacks do not emerge from the problem itself but from the values of the dimensionless numbers that Henry had to use to solve the problem semianalytically and that have been used by most researchers ever since. *Simpson and Clement* (2004) proposed reducing the value of the a parameter (dimensionless freshwater flux). Here we propose reducing the b parameter (Peclet number). The resulting problem is sensitive to density variations within the domain and thus more appropriate for testing seawater intrusion codes where stable density profiles extend throughout most of the domain. A second feature of the reduced diffusion problem is a seawater intrusion wedge that is consistent with widely accepted concepts. That is, seawater flows subhorizontally towards the mixing zone where it is carried back seawards by the inland freshwater discharge. Moreover, concentration profiles are similar to those observed in the field.

However, we propose the use of an alternative that accounts for velocity dependent dispersion and anisotropic hydraulic conductivity. This dispersive Henry problem provides a valuable tool for gaining insight into the mechanisms controlling seawater intrusion into coastal aquifers. As with the diffusive Henry problem, the dispersive version leads to a wedge where seawater flows horizontally towards an inclined mixing zone, salt disperses into the outflowing freshwater, so that its density is reduced, causing it to float upwards. As it mixes with freshwater essentially by transverse dispersion, it is carried back to sea leading to the convection cell displayed in Figure 2.14.

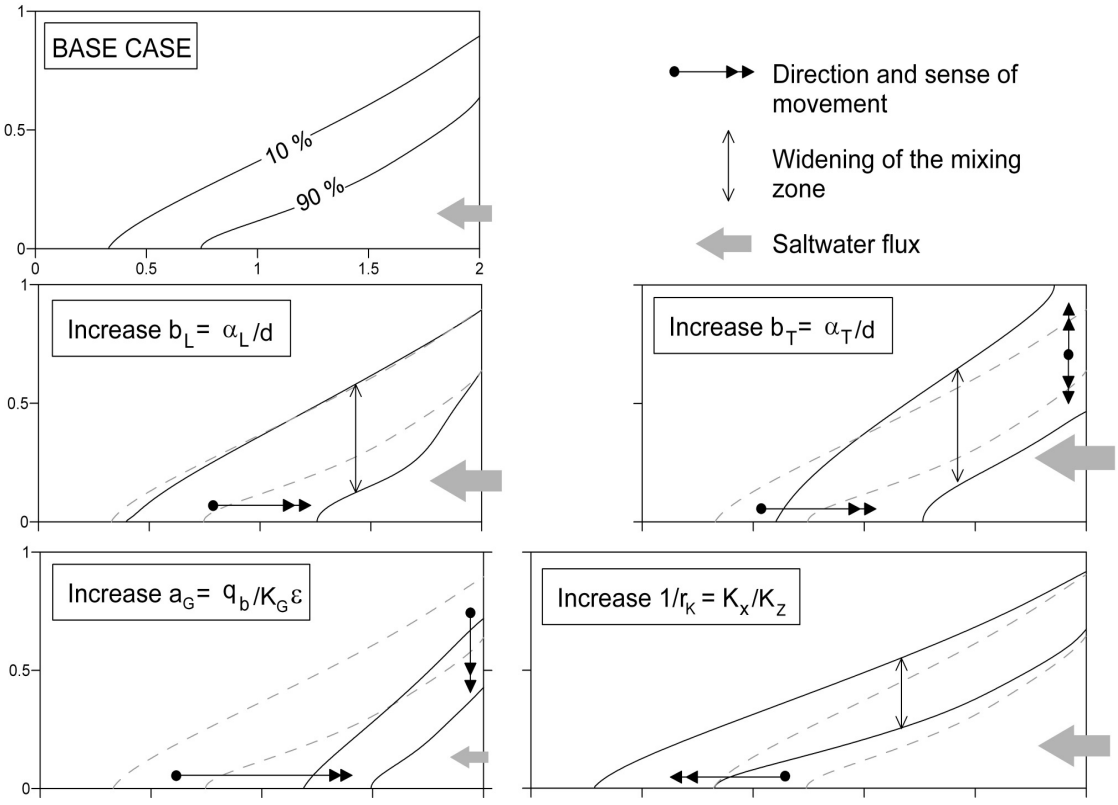

Figure 2.14: Qualitative behavior of the solution to the dispersive Henry problem. As longitudinal dispersivity increases, so do seawater flux and the width of the mixing zone, whose saline end moves seawards. Increasing transverse dispersivity broadens and tilts the mixing zone, while also increasing seawater flux. Increasing the dimensionless freshwater flux pushes the mixing zone seawards whereas an increase in the ratio k_x/k_z pushes it landwards.

We summarize the behavior of the solution in terms of three outputs variables: toe penetra-

tion, width of the mixing zone and saltwater flux. To this end, we first performed a dimensional analysis to identify the governing parameters and chose as dimensionless parameters those of the original Henry problem: a, dimensionless freshwater flux (relating viscous and buoyancy forces) and b, Peclet number, which we denote by b_L when diffusive mixing is substituted by dispersive mixing. Two new dimensionless parameters emerge: r_α and r_K, anisotropy ratios for dispersivity and hydraulic conductivity, respectively.

Toe penetration L_D is described qualitatively by the Ghyben-Herzberg approximation (e.g. *Bear* (1972)). L_D increases with hydraulic conductivity and decreases with freshwater flux. As seawater flux causes a seawater head loss, the saltwater wedge recedes with increasing dispersion (i.e. L_D decreases). Longitudinal and transverse dispersion contribute in a similar amount. Deviations with respect to L_{GH} depend on the geometric average of dispersivities.

The width for the dispersive case is quite constant along the mixing zone and is controlled basically by $\alpha_G = \sqrt{\alpha_L \alpha_T}$. Therefore, the contribution of longitudinal and transverse dispersivity to the width is comparable, which is somewhat surprising because concentration isolines throughout most of the mixing zone are parallel to the water flux. Therefore, one might expect transverse dispersion to control the width. As it turns out, the areas where the salinity gradient is not parallel to the water flux (near the toe and the saltwater side of the mixing zone) appear to contribute as much to the width of the mixing zone as the rest. While the contribution of the two dispersivities is quantitatively similar, they affect the concentration profile in a different way. Transverse dispersivity contributes to broadening the concentration profile throughout the domain. Increasing longitudinal dispersivity, on the other hand, leads to seawards displacement of the high concentration isolines, leaving the freshwater end unaffected. As a result, vertical concentration profiles still display a sharp concentration increase at the mixing zone but leading to concentrations well below seawater (75 to 90%). Since this feature is frequently observed in actual salinity logs, we infer that longitudinal dispersivity may exceed transverse dispersivity by much more than the traditional factor of 10. High sensitivity of width to dispersivities is especially relevant because these

parameters are usually hard to characterize, while the width of the mixing zone can be measured. This finding implies that the width can be used to derive field values of dispersivity.

Saltwater flux across the seaside boundary is basically proportional to K_G (geometric average of the principal hydraulic conductivities) times the cubic root of the transverse dispersivity. These parameters are similar to the obtained by *Smith* (2004). Saltwater flux is usually considered small compared to the freshwater flux. The extreme case is the sharp interface approximation that neglects saltwater circulation. However, saltwater fluxes computed here are of the order of 10 to 90% of the freshwater flux. An accurate quantification of the saltwater mass flux is important for reactive transport processes in the mixing zone and should be subject of special attention in seawater intrusion studies.

Results show that some of the key factors controlling the studied variables are not explicitly present in the dimensional analysis of Section 2.3.2. The geometric means of hydraulic conductivity and dispersivity coefficients should appear in the dimensionless numbers, being a_G a better expression for the relationship between viscous and buoyancy forces and b_G or b_L better expressions of the Peclet number. The effect of those factors is synthetically summarized in Figure 2.14.

Chapter 3

Seawater intrusion through heterogeneous aquifers

3.1 Introduction

Heterogeneity in hydraulic properties, especially hydraulic conductivity, is well known to significantly affect groundwater flow and solute transport. In variable density flow systems, heterogeneity can perturb flow over many length scales, ranging from slight differences in pore geometry to larger heterogeneities at the regional scale. Yet, few studies have focused on evaluating the impact of heterogeneity on variable density flow. As pointed out by *Simmons et al.* (2001), there are many unanswered questions in understanding variable density flow and solute transport in heterogeneous porous media.

Different set-ups can be considered in density dependent flow: unstable configurations (sinking of a denser plume) and stable configurations (seawater intrusion). Most of recent studies regarding the effect of heterogeneity in density dependent flow deal with unstable configurations. In this context, *Mc Kibbin and O'Sullivan* (1980); *Mc Kibbin and Tyvand* (1982, 1983) have investigated

the effect that multiple hydraulic conductivity layers have on thermal convection. Experimental investigations of variable-density groundwater flow in homogeneous, layered, and lenticular media showed that dense water tends to accumulate along bedding interfaces (*Schincariol and Schwartz*, 1990). These findings have been modelled by simulating heterogeneity in the hydraulic conductivity (*Schincariol and Mendoza*, 1997; *Schincariol*, 1998). Their results show that the statistical characteristics of the permeability field (mean, variance, and correlation length) play a critical role in the onset and subsequent growth or decay of gravitational instabilities. Specifically, homogeneous field criteria for perturbation initiation are not applicable for local-scale heterogeneities *Schincariol* (1998). In fact, the presence of instabilities is intimately related to the structure and variance of the permeability field *Simmons et al.* (2001). Not surprisingly, ordered heterogeneities with vertically oriented high-permeability regions tend to enhance growth conditions while horizontal elongated structures (stochastic distribution) tend to dissipate free convection through dispersive mixing.

Unfortunately, the above studies do not apply to the study of saltwater intrusion processes since they focus on instabilities caused by dense fluids overlying lighter ones. Few investigations have been devoted to the study of the heterogeneity in coastal aquifers. *Schwarz* (1999) studied the effect of heterogeneity for some of the most typical benchmarks problems for density dependent flow, including the Henry Problem for saltwater intrusion. This work was recently continued by *Held et al.* (2005). They performed a theoretical and numerical analysis of heterogeneity in seawater intrusion problems. The theoretical analysis is based on the homogenization theory to derive effective flow and transport parameters for statistically isotropic and anisotropic heterogeneous permeability fields. Their approach is similar to that of *Welty and Gelhar* (1991) and *Welty et al.* (2003). *Held et al.* (2005) found that for isotropic media the effective permeability corresponds to the geometric mean, as in non-density dependent flow problems. For the anisotropic case, they found expressions for the anisotropic effective permeability for Gaussian log normal permeability distributions equal to the expression of *Gelhar and Axness* (1983) for uniform density flow. However, their theoretical analysis is based on uniform density driven flow in a infinite medium,

thereby neglecting the role of boundary conditions, which condition flow in seawater intrusion problems to the point that density variation within the domain can sometimes be ignored (*Simpson and Clement*, 2003).

3.1.1 Scope and objectives

The objective of this work is (1) to assess the effect of heterogeneity on the steady state position of the saltwater intrusion wedge and (2) to analyze whether it can be approximated by a homogeneous equivalent medium. Specifically, we seek if such approximation can reproduce the main features: the interface penetration, the width of the mixing zone and the amount of saltwater that enters the aquifer. To this end, we perform random realizations of heterogeneous permeability fields using different variograms to assess the role of heterogeneity scale (correlation length) and the permeability contrast (variance). Since small and medium scale heterogeneities of natural media are in general not properly represented in numerical models, we study the impact of these simplification in seawater intrusion modelling.

A small correlation length allows us to evaluate the effect of small scale heterogeneity and suggests ergodicity of the random realizations. To assess the effect of medium scale heterogeneities in real aquifers, we considered a longer correlation length. Large scale heterogeneities have not been studied here. Such heterogeneities need to be characterized by geological studies and should be explicitly represented in the model.

3.2 Methodology

We approach this problem from a numerical perspective. As in the previous Chapter, we consider here two basic cases: a purely diffusive and a purely dispersive case. Boundary conditions and flow and transport parameters used have been discussed in Chapter 2 and are shown together with the model domain in Figure 2.1.

3.2.1 Study of the effect of heterogeneity in Seawater Intrusion

Series of 50 random permeability fields were generated using the GCOSIM3D code of *Gomez-Hernandez and Journel* (1993). Hydraulic conductivity is chosen to follow a log-normal probability density function. Spatial variability is characterized by a spherical variogram with anisotropic correlation lengths. Different correlation lengths (λ) and variances (σ^2_{lnK}) have been used to study the effect of heterogeneity scale and permeability contrast (Table 3.1).

Table 3.1: Geostatistical description of all cases studied (lengths are scaled by the aquifer thickness)

Scale	λ_x	λ_y	Grid	σ^2_{lnK}
Short	0.045	0.015	257 x 257	1
Short	0.045	0.015	257 x 257	2
Long	0.15	0.045	257 x 129	1
Long	0.15	0.045	257 x 129	2

Density dependent flow and solute transport simulations were carried out with the SUTRA code (*Voss and Provost*, 2002) to obtain the steady state position of the freshwater/seawater mixing zone. The discretization depends on the considered heterogeneity scale and is adjusted to provide a sufficient resolution to represent the random permeability fields while ensuring the stability of the solution.

Simulation results are analyzed in terms of the same characteristic output variables as in the previous Chapter:

- $L_D = L_{toe}/d$ (Dimensionless toe penetration) L_{toe} is the penetration length of the seawater intrusion wedge, measured as the distance between the seaside boundary and the point where

the 50% mixing isoline intersects the aquifer bottom (see Figure 2.3) and d is the aquifer thickness.

- W_D (Dimensionless averaged width of the mixing zone) is computed by averaging WMZ/d, where WMZ is the vertical distance between isoconcentration lines of 25% and 75% mixing ratios. In order to avoid boundary effects, averaging is restricted to the interval between $0.2L_D$ and $0.8L_D$ (see Figure 2.3).

- $R_D = SWMF/q_b\, d$ (Dimensionless saltwater flux) $SWMF$ is the saltwater flux that enters the system across the seaside boundary (kg/s/m) integrated over the inflowing portion of the domain. Therefore, R_D is the ratio between the volumetric flow rates of inflowing seawater and freshwater.

3.2.2 Are there any effective parameters for flow and transport?

Considering the resulting heterogeneous simulations as the "true" solution for each realization, we seek to determine whether they can be reproduced by a homogeneous equivalent representation. To this end, we find first the components of the effective permeability tensor and then the effective dispersion/diffusion coefficients.

Evaluation of the effective and equivalent horizontal and vertical permeabilities

There are many possible methods to evaluate representative hydraulic conductivity for groundwater flow (*Renard and de Marsily*, 1997; *Sanchez-Vila et al.*, 2006). Here, two representative homogeneous permeability tensors are evaluated. First, we compute an effective permeability tensor for each considered variogram, and second, we compute the equivalent permeability tensor for each realization.

There is, up to now, no analytical expression to evaluate the effective permeability in a den-

sity dependent and bounded flow problem. *Welty et al.* (2003) have studied dispersive mixing in concentration-dependent transport in three-dimensional, anisotropic heterogeneous porous media, evaluated the principal components of the effective permeability tensor using equation (53) of *Gelhar and Axness* (1983). *Held et al.* (2005) obtained the same expression as *Gelhar and Axness* (1983) by means of homogenization theory for a density dependent flow problem in an unbounded domain. Therefore, we can use *Gelhar and Axness* (1983) expression as a first approximation of the effective permeability tensor.

$$K_{eff,i} = K_G \left[1 + \sigma^2_{lnK}\left(\frac{1}{2} - \frac{\lambda_j}{\lambda_1 + \lambda_2}\right)\right] \qquad \text{with } i, j = 1, 2 \text{ and } i \neq j \tag{3.1}$$

This approach is only valid for small correlation lengths that ensure ergodicity. In those cases, a unique effective permeability tensor can be considered representative for all realizations obtained with a given variogram.

The components of the equivalent permeability tensor for each realization were obtained using the Darcian approach, which is equivalent to most others (*Sánchez-Vila et al.*, 1993). The horizontal equivalent permeability is the one yielded the same flux for uniform horizontal field and the corresponding definition applies for the vertical permeability (Figure 3.1).

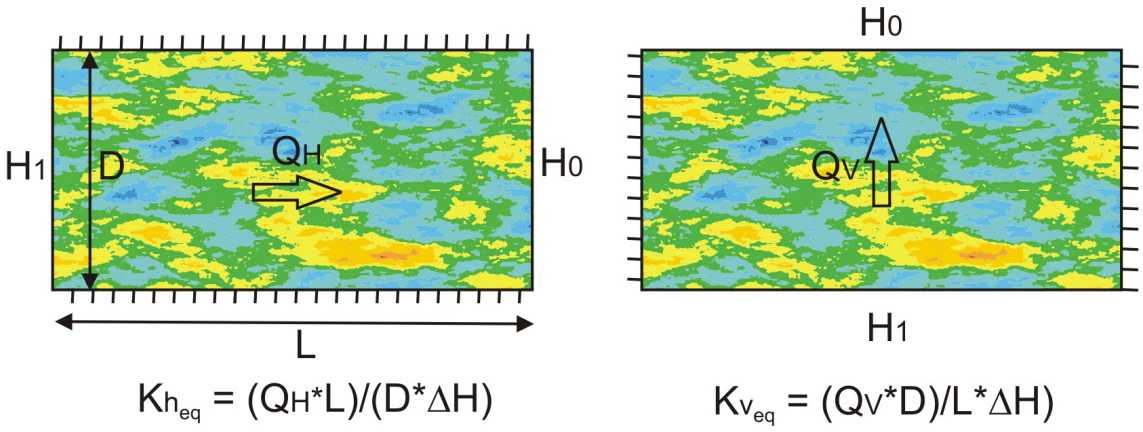

Figure 3.1: Scheme of numerical set-ups to obtain K_{Heq} and K_{Veq}

The assumption of uniform flow is not strictly valid in the seawater intrusion context. Yet, the results of *Held et al.* (2005) suggest that it is a valid option. The resulting equivalent permeability tensors are different for each realization. Differences are small for cases of short correlation lengths and small variance, but may reach order of magnitude values in cases of large correlation distance and high variance. We used them to represent a possible homogeneous anisotropic media.

Evaluation of the effective dispersion

The local dispersion used in the heterogeneous simulations are those of the dispersive anisotropic Henry problem presented in the previous chapter, i.e., $\alpha_L = 0.1$ and $\alpha_L = 0.01$. These values can be considered too large for representing local dispersion in steady flow. However, temporal fluctuations caused by tidal and wind effects are known to significantly increase dispersion (*Dentz and Carrera*, 2003; *Cirpka and Attinger*, 2003; *Dentz and Carrera*, 2005). As a result, local dispersivity values are high compared to the simulated degree of heterogeneity which restricts the applicability of macrodispersion concepts. *Gelhar and Axness* (1983) expression of the macrodispersion tensor for anisotropic 2D media, is only valid for $\alpha_L/\lambda \ll 0.01$. In our case, $\alpha_L/\lambda > 0.5$, resulting in a highly dispersive problem and invalidating its use.

More appropriate is the application of the effective longitudinal and transverse expressions obtained by means of perturbation theory (*Dentz et al.*, 2000) for transport in heterogeneous media. The method, still, has some limitations for its application to the present work. First, the analysis is based on constant local dispersion coefficients, $D_L = \alpha_L \bar{u}$, $D_T = \alpha_T \bar{u}$ with $\bar{u}$ the mean velocity, which is aligned with the 1-direction. Thus, it is rather 'anisotropic diffusion' than real dispersion. Therefore it would be appropriate to represent the diffusive interface rather than the dispersive interface. Despite this fact, we consider it as a first approximation for the effective dispersion parameters. Moreover, the density dependent code we are using, SUTRA, does not allow for the implementation of anisotropic diffusion coefficients, and therefore those values are not applicable to the diffusive case. Second, the expressions for the effective dispersion coefficients are based

on second order perturbation theory in the fluctuation of the random velocity field and thus are strictly valid only for moderate heterogeneity, i.e., ${\sigma_{lnK}}^2 \ll 1$.

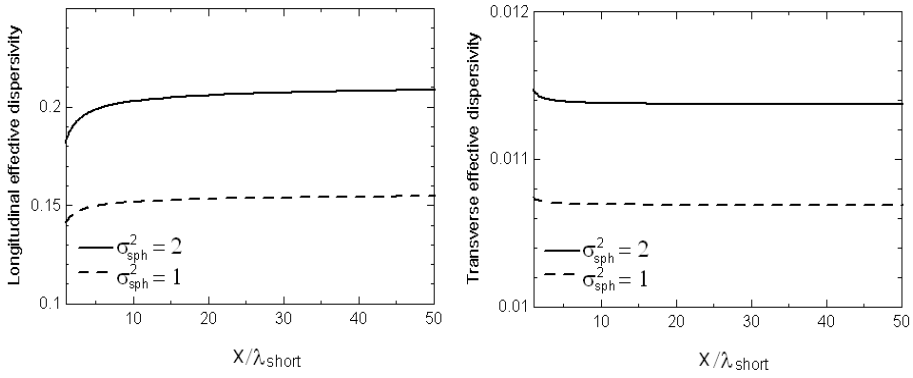

Figure 3.2: Longitudinal and transverse effective dispersivity obtained by means of the perturbation theory (*Dentz et al.*, 2000) for short correlation distances ($\lambda_x = 0.045$ and $\lambda_y = 0.015$)

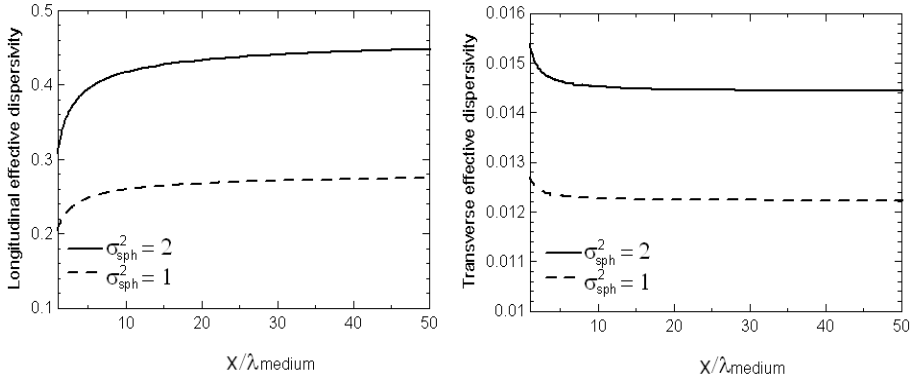

Figure 3.3: Longitudinal and transverse effective dispersivity obtained by means of the perturbation theory (*Dentz et al.*, 2000) for medium correlation distances ($\lambda_x = 0.15$ and $\lambda_y = 0.045$)

Dentz et al. (2000) computed effective dispersivity values for a Gaussian correlation function. To be able to work with those expressions, first we need to compute the correlation lengths and disorder strength for the Gaussian model that correspond to the ones for the Spherical correlation function. To this aim, the zeroth moment and the normalized second moment of the two correlation functions are compared. This implies the relations $\lambda_{Gauss} = \sqrt{\frac{64}{175}}\lambda_{sph}$ and ${\sigma_{Gauss}}^2 = 1.71\,{\sigma_{sph}}^2$. With those values, the following curves (Figures 3.2 and 3.3) for the effective dispersion coefficients are computed.

In this study, we assume that the observation length (x) used to evaluate the typical effective dispersion coefficients is the L_{toe} of the heterogeneous simulations.

3.3 Qualitative effect of heterogeneity in seawater intrusion

Here, we study the impact of heterogeneity on the shape and size of the mixing zone for selected simulations. The concentration distribution for some medium scale heterogeneous realizations are shown in Figure 3.4 for both the dispersive and diffusive cases.

Some patterns that appear in this solution are general for all the results, although the effect is more evident in the dispersive simulations:

- As expected, the slope of the interface is low in the high permeability zones, whereas it increases in the low permeability zones.
- Central isolines (30-70% mixing lines) tend to accumulate in high permeability zones while they tend to spread out in low permeability zones. For this reason, those isolines seem to accommodate under high permeability areas. This effect is smoothed for the isolines corresponding to very high or very low salt mass fraction.
- High permeability zones located at the mixing zone cause channeling of outflowing freshwater.

Figure 3.5 shows the interface in a random permeability field and the interface for a homogeneous medium with the same equivalent horizontal and vertical permeability as the random field. Also shown is the vertically integrated water flux over the seaside boundary. Obviously, the upper value coincides with the flow rate prescribed at the freshwater boundary. In the homogeneous medium, the maximum positive value indicates where the change in the flow direction takes place

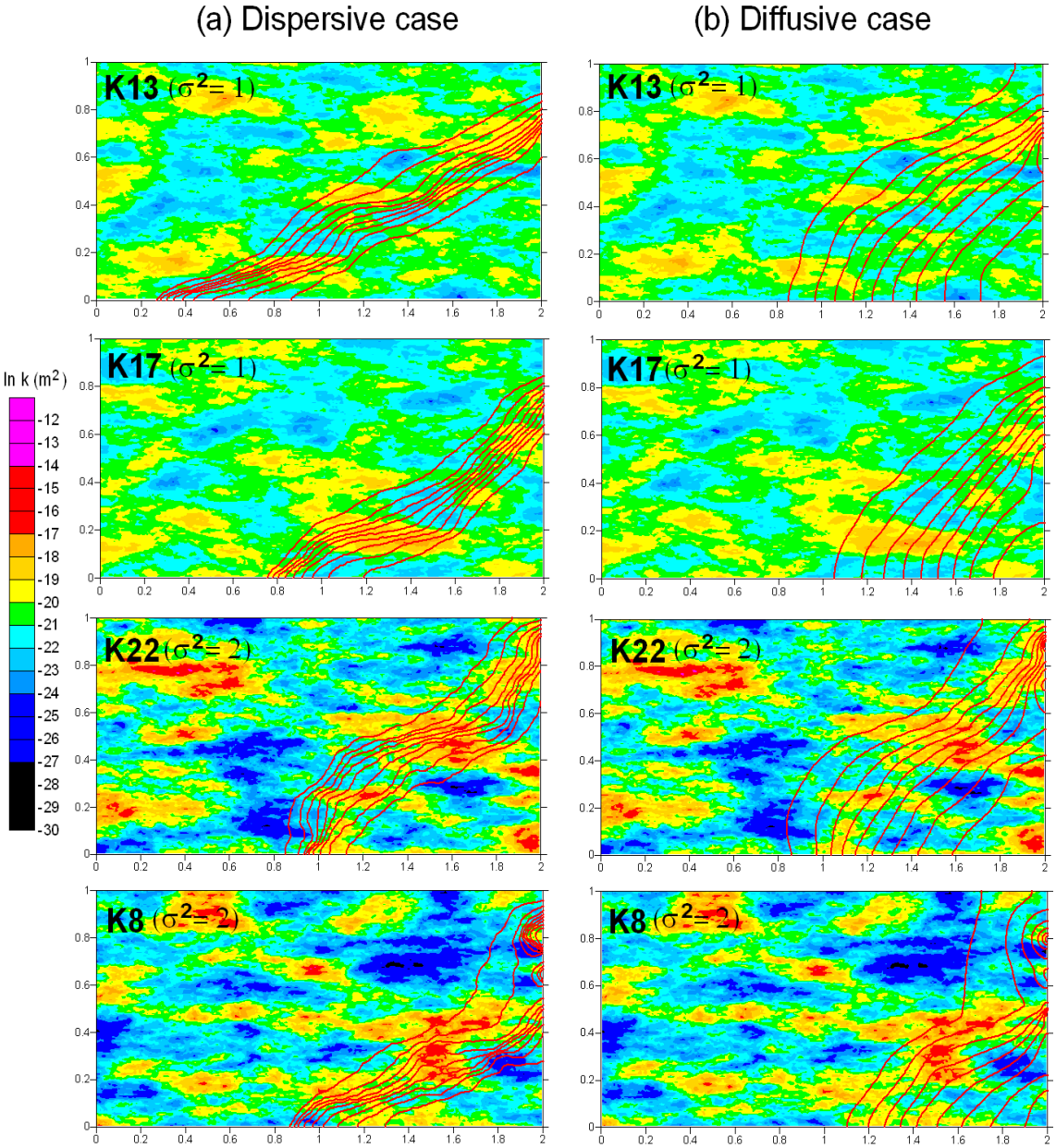

Figure 3.4: Seawater intrusion wedge, as characterized by the mixing isolines (0.1 to 0.9 isolines from top to bottom), computed for typical realizations of k with λ_{medium} and $\sigma^2 = 1$ (K13 and K13) or $\sigma^2 = 2$ (K8 and K22) for both the dispersive and diffusive transport problems

(from this point water flows out of the system). This point is lower in the diffusive than in the dispersive homogeneous case.

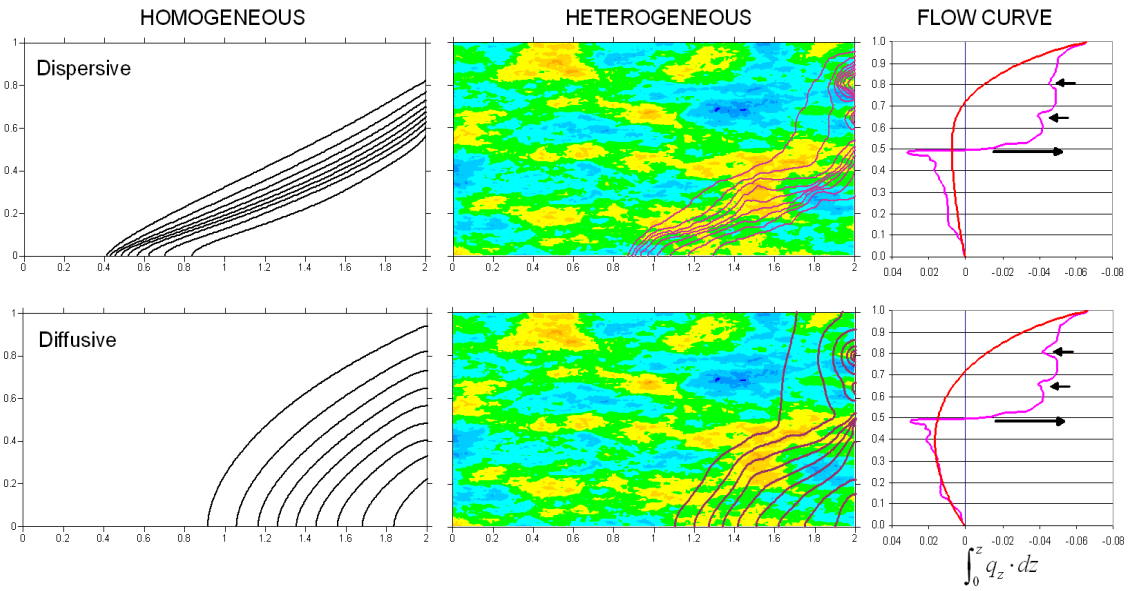

Figure 3.5: Comparison between the freshwater/saltwater mixing zone in an homogenous and a heterogeneous medium with the same effective permeability. The interface is shown for a dispersive and a purely diffusive heterogeneous case. On the right a plot vertically integrated flux along the seaside boundary ($\int_0^z q_z dz$) is shown for the homogeneous (red) and the heterogeneous case (pink). Positive values indicate incoming water and negative values outflowing.

However, when we look at the integral for the heterogeneous cases, we observe that:

- The shape and magnitude of the flow curve is similar for both the dispersive and diffusive cases, implying the saltwater fluxes in heterogeneous media to be controlled by the permeability distribution rather than by the diffusion/dispersion processes.

- High permeability zones located in the mixing zone and well connected to the freshwater zone cause freshwater channeling towards the sea. In the case represented in Figure 3.5, the zone represented by the arrow pointing right, flushes almost completely the saltwater that has entered below it.

- High permeability regions within the mixing zone that are poorly connected to the flowing freshwater (two small arrows pointing left in Figure 3.5) produce local circulation cells that slightly affect the overall shape of the interface.

3.4 Small scale heterogeneity

Small scale heterogeneities are much smaller than the typical length of the studied phenomenon, in this case, the interface penetration length. We use them to represent the effect of small scale variability that is present in all natural media but cannot be explicitly included in numerical models. Two different variograms are considered with an increase in the degree of heterogeneity, i.e., with two different values of σ^2_{lnK} (see Table 3.1).

3.4.1 Medium variance ($\sigma^2 = 1$)

Figure 3.6 displays the interface shape and position in some heterogeneous realizations including dispersion and diffusion as local mixing mechanism.

The isolines are locally affected by the small scale variability resulting in slightly wavy isolines. The effect is smoothed in the diffusive interfaces. At first sight, the overall affect of this small scale heterogeneity does not seem to be critical for the representation of the general features of the freshwater/saltwater interface.

Effective and equivalent permeability

We used *Gelhar and Axness* (1983) expression as a first approximation of the effective permeability tensor. Since $x/\lambda \simeq 33$, we expect the ergodic solution to be fully applicable in this case, at least at some distance from the boundary. The computed values of $K_{eff,1}$ and $K_{eff,2}$, in m/d, are:

$$K_{eff,1} = 1.25\, K_G = 1080\ m/d \qquad \text{and} \qquad K_{eff,2} = 0.75\, K_G = 648\ m/d \tag{3.2}$$

The interface obtained with these and with equivalent permeabilities and local dispersion/ diffusion are depicted in Figure 3.7 and 3.8 (diffusive and dispersive case, respectively). The solution

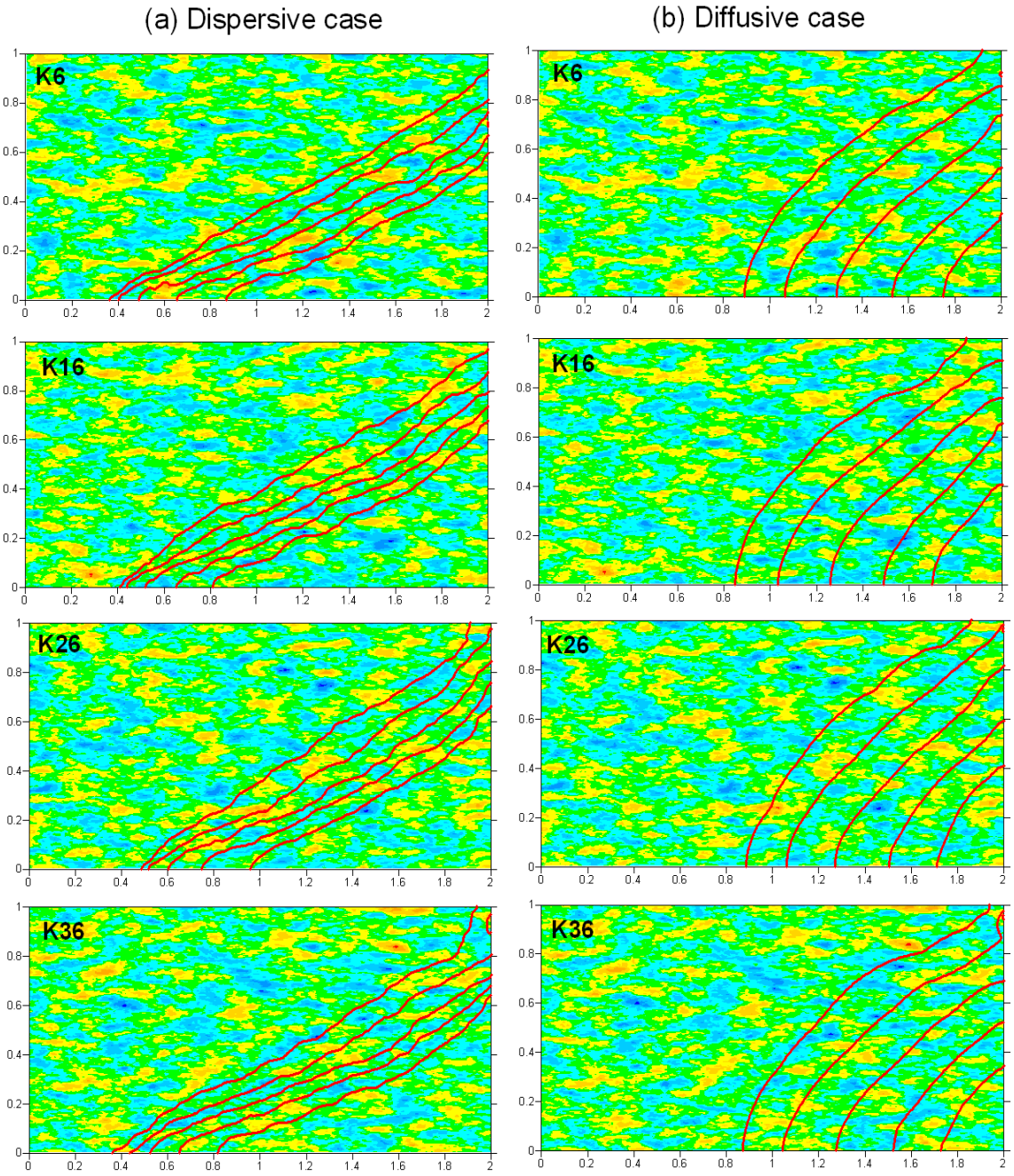

Figure 3.6: Seawater intrusion wedge, as characterized by the mixing isolines (0.1, 0.25, 0.5, 0.75 and 0.9 isolines from top to bottom), computed for typical realizations of k (6,16,26 and 36) with short λ and $\sigma^2 = 1$ for both the dispersive and diffusive transport problems.

of the effective medium is compared with two different heterogeneous simulations. As expected, differences between the effective and equivalent permeabilities are minor and the results obtained for the homogeneous medium with local dispersion compare well with those of the heterogeneous medium. Local perturbations are not reproduced but the toe position and the width of the mixing zone are fit fairly well. For the diffusive case, the result that an homogeneous media with effective permeability and the local diffusion coefficient offers a good representation of the heterogeneous realizations agrees with the results by *Held et al.* (2005) for a variogram similar to the one considered here.

Effective diffusion and dispersion

Results obtained with local dispersivity or diffusion coefficient, display some common features, more evident in some realizations than in others. At the bottom of the aquifer, the heterogeneous media interfaces move slightly seawards and, at the top part (near the seaside boundary), upwards. Both displacements result in the rotation of the interface. This slight rotation of the interface could be reproduced by an increase in the transversal dispersion of the equivalent homogeneous media, as described in Figure 2.14 of previous chapter. These results suggest that heterogeneity slightly increases dispersion.

We applied the effective longitudinal and transversal expressions from *Dentz et al.* (2000) as a first approximation to the effective dispersion coefficients. We assumed that the observation length (x) used to evaluate the effective dispersion coefficients equals the toe distance of the heterogeneous simulations. As observed in Figure 3.6, this length is about 1.6 m in the considered realizations. The effective dispersion coefficients obtained by means of the curves in Figure 3.2 for $x/\lambda_x = 35.5$, are:

$$\alpha_{Leff} = 0.1561 \qquad \alpha_{Teff} = 0.0107 \tag{3.3}$$

These effective values cannot be considered "macro" since the increase in the longitudinal

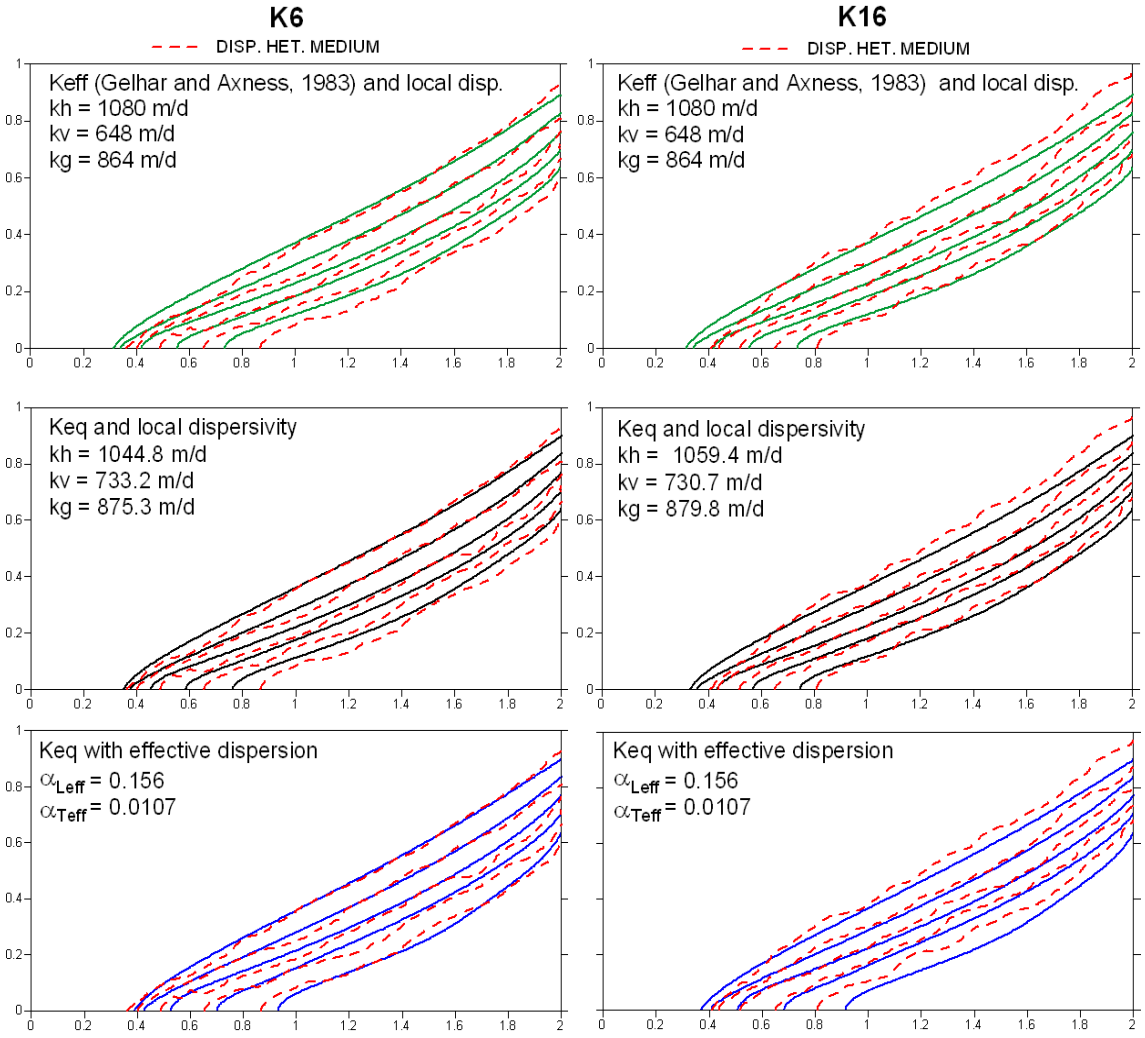

Figure 3.7: Dispersive solution of two heterogeneous realizations with short λ and $\sigma^2 = 1$ (dashed lines) compared to the solution of three different homogeneous media. The parameters used are indicated in each case.

dispersively coefficient is of the same order of magnitude as the local value. In general,, this slight increase improves the fit between the heterogeneous and homogeneous media (Figure 3.7). The seawards displacement in the toe position is well matched by the effective parameters. However, the upwards movement of the interface is not reproduced. This fact is due to the small increase in the effective transverse value with respect to its local value. This implies that heterogeneity affects transverse dispersion more than what would be expected from the perturbation theory expressions

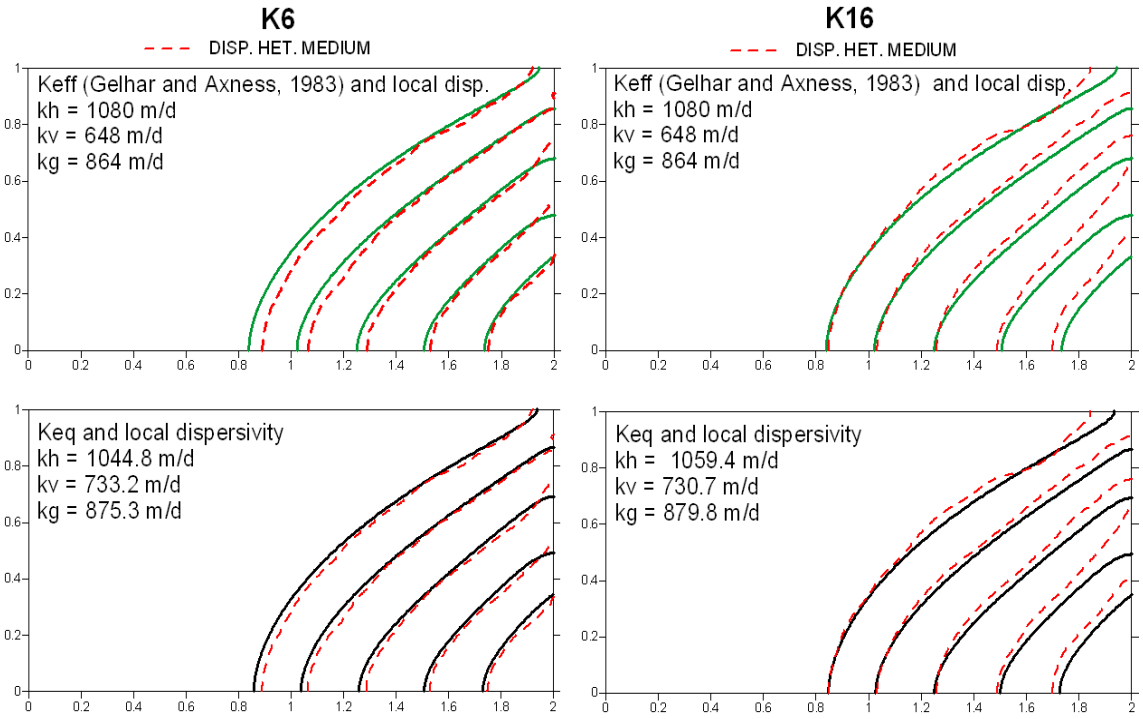

Figure 3.8: Diffusive solution of two heterogeneous realizations with short λ and $\sigma^2 = 1$ (dashed lines) compared to the solution of three different homogeneous media. The parameters used are indicated in each case.

for effective dispersivity.

In summary, for the case of small scale heterogeneity with $\sigma^2 = 1$, the effect of heterogeneity is not strong and all the possible effective media considered offer a fairly good representation of the heterogeneous solutions. Among them, the best fit is obtained for either a medium of equivalent permeability or the effective permeability and the effective dispersion tensor obtained with perturbation theory.

Ensemble

The ensemble of concentrations of the 50 heterogeneous simulations is presented in Figure 3.9. The ensemble is compared with the solution of the homogeneous medium with local dispersion/diffusion coefficients. It offers a fairly good representation of the ensemble of concentrations

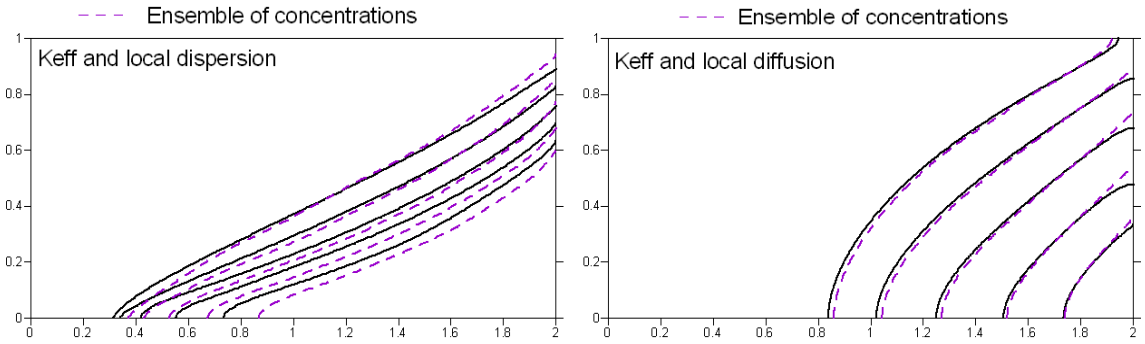

Figure 3.9: Ensemble of concentrations of the 50 heterogeneous realizations with short λ and $\sigma^2 = 1$ (dashed lines) for the dispersive and diffusive case compared to the solution of a homogeneous medium with K_{eff} and local dispersion/diffusion

of small scale heterogeneous realizations with $\sigma^2 = 1$. However, unlike for the homogeneous dispersive case, isolines in the ensemble are displaced upwards as in each single heterogeneous realization, whereas the toe moves seawards, which again results in the rotation of the interface. Therefore, the need of an increase in the transverse dispersivity is again suggested. A best solution is obtained with the effective dispersion coefficients (Figure 3.10). These parameters provides

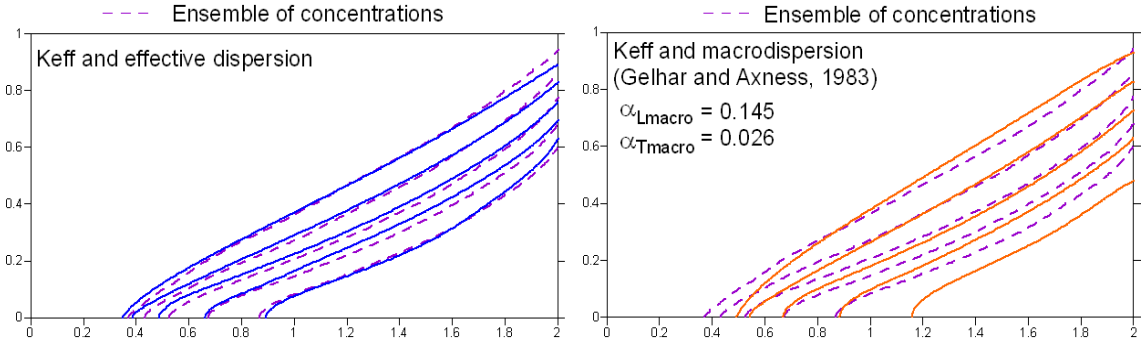

Figure 3.10: Ensemble of concentrations of the 50 heterogeneous realizations with short λ and $\sigma^2 = 1$ (dashed lines) for the dispersive case compared to the solution of a homogeneous medium with K_{eff} and (1) effective dispersion coefficients or (2) macrodispersion

a satisfactory representation of the mean behavior of seawater intrusion in moderately heterogeneous media. The solution obtained with the macrodispersion tensor calculated following *Gelhar and Axness* (1983) expressions shows that macrodispersion overestimates the with of the mixing zone and underestimates the toe penetration. This result agrees with that of *Held et al.* (2005).

This result can be attributed either to the application of macrodispersion in a case of small Peclet numbers, as explained before, or to the decrease in the value of macrodispersivity as the magnitude of the concentration gradient increases (*Schotting et al.*, 1999).

3.4.2 Large variance ($\sigma^2 = 2$)

A larger contrast in the permeability fields, i.e., increasing the variance of *lnk*, leads to a marked effect in the interface shape. Some solutions for the dispersive and diffusive cases are depicted in Figure 3.11.

In an anisotropic medium, the equivalent horizontal permeability increases with increasing variance whereas the vertical permeability is reduced. The toe location is mainly controlled by the horizontal permeability (see previous chapter). Since the Henry problem domain is very restrictive to changes in permeability, a large increase in K_H may lead to boundary effects in the solution of the interface position. For this reason, we have scaled the heterogeneous fields so that their horizontal equivalent permeability is equal in all the realizations. This scaling causes a modification in the statistical properties of the ensemble. The σ^2_{lnK} is maintained whereas the mean value of the log-permeability field is modified by a factor of $\epsilon = K_{Htarget}/K_{Heq}$. We aim at comparing each heterogeneous realization with each corresponding equivalent medium, in which case this scaling does not affect the comparison. However, the ensemble average over the different heterogeneous realizations is not representative as the mean value of *lnk* varies from realization o realization. This is of minor concern because each simulation is so different that it is clear we are far from ergodicity.

Effective parameters

In Figure 3.12 the mixing zones of two heterogeneous media are compared to (1) a medium with K_{eq} and local dispersivity values and (2) a medium with K_{eq} and effective dispersion values. Figure

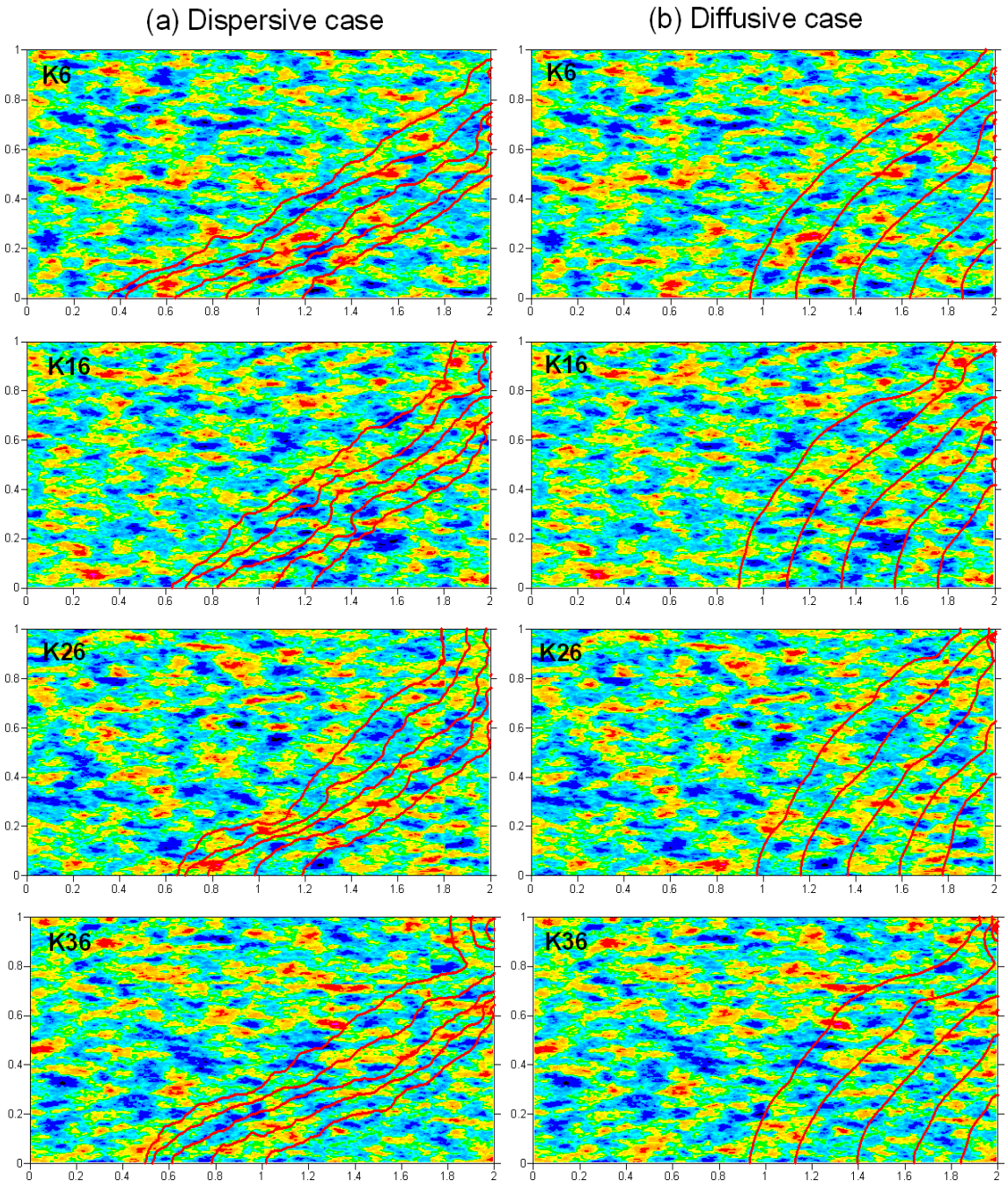

Figure 3.11: Freshwater/saltwater mixing zones in some heterogeneous media with short λ and $\sigma^2 = 2$.

3.13 shows the diffusive mixing zone of two heterogeneous media compared to a medium with K_{eq} and the local diffusion coefficient. The medium with local dispersion does not reproduce properly the heterogeneous solution. In all the simulations, the toe position (50% of seawater concentration at the aquifer bottom) is overestimated, the width of the mixing zone underestimated, and the slope of the interface is not well reproduced. This comparison reflects the necessity for a higher value of the dispersion to represent these media, in particular in transverse dispersion. The variability in the slope of the heterogeneous simulations (Figure 3.11) suggests that the effective transverse dispersivity depends on the realization and that this value presents larger fluctuations than the longitudinal dispersivity. As a first approximation to the effective dispersivity values we used the values obtained by means of the perturbation theory. These values are considered valid for $\sigma^2 \ll 1$, its application to variances as large as 2, as in this case, should be seen as a first approximation of the effective dispersion values.

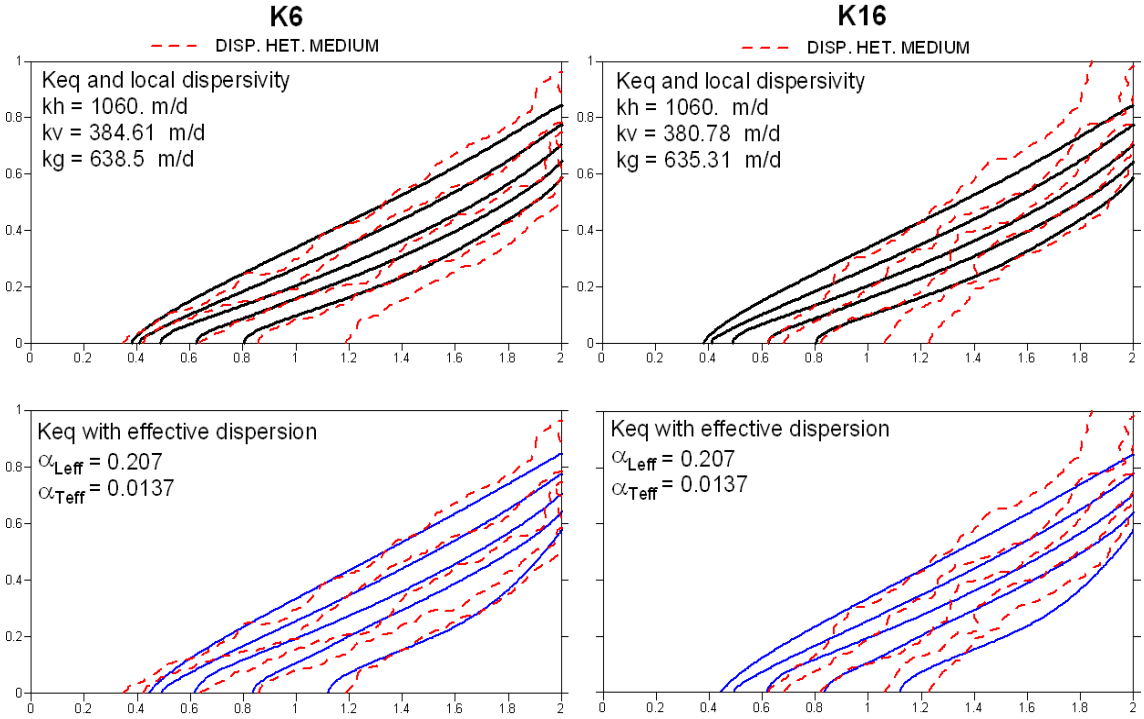

Figure 3.12: Isoconcentration lines for two heterogeneous realizations with short λ and $\sigma^2 = 2$ (dashed lines) compared to a medium two homogeneous medium, one with local and the other with effective dispersivity coefficients.

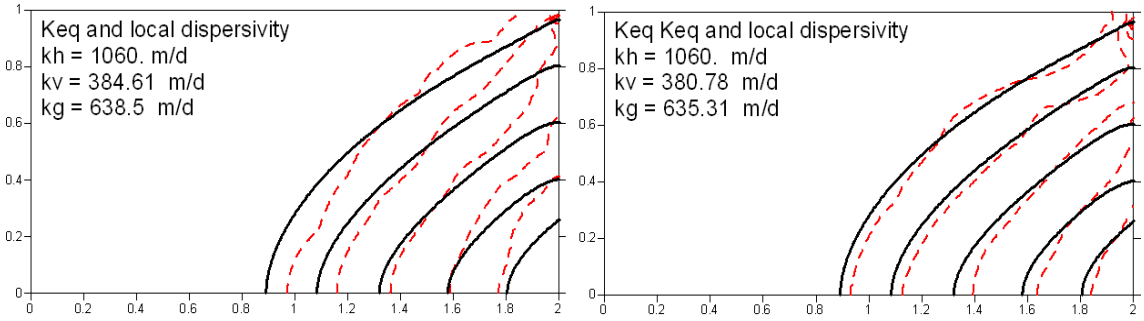

Figure 3.13: Diffusive interface (dashed lines) for two heterogeneous realizations with short λ and $\sigma^2 = 2$ compared to an homogenous medium with the local diffusion coefficient.

The effective dispersion is determined by means of the curves presented in Figure 3.2. For the two cases presented in this Figure we obtain:

$$\begin{aligned} K6 \quad & \frac{x}{\lambda_x} = 30.66 \quad \alpha_{Leff} = 0.207 \quad \alpha_{Teff} = 0.0137 \\ K16 \quad & \frac{x}{\lambda_x} = 26.66 \quad \alpha_{Leff} = 0.207 \quad \alpha_{Teff} = 0.0137 \end{aligned} \tag{3.4}$$

As shown in Figure 3.12, the increase in the longitudinal dispersivity induces a seawards displacement of the toe, thereby improving the representation of the mixing zone near the aquifer bottom. However, as for the medium variance case, the upwards movement is not well reproduced either by local dispersivity values nor by the effective parameters, suggesting that the value of the transverse dispersivity is underestimated by the perturbation theory values.

3.5 Medium scale heterogeneity

We analyze now the presence of heterogeneities which are medium to large compared with the domain size. An example would be the presence of lenticular bodies of different permeabilities that are not considered different aquifers because there are not laterally continuous. The correlation lengths considered are large enough to jeopardize the possibility of achieving ergodic conditions, and thereby stochastic approaches may not be appropriate to evaluate effective parameters for these

heterogeneous media. Although we are not able to quantify the effect of heterogeneity, we aim to qualitatively determine if neglecting medium scale heterogeneities is critical to represent seawater intrusion and whether results are consistent with those of small scale heterogeneity. Again, we evaluate the effect of two different values of σ^2_{lnK}.

3.5.1 Medium variance ($\sigma^2 = 1$)

Results for this case were presented in Section 3 (Figure 3.4). Results show a high variability in terms of the toe penetration. The mixing zone has an irregular width, in general wider than for short correlation. However, this widening has not a common pattern i.e., it does not affect always the same location.

Effective parameters

Figures 3.14 and 3.15 display two heterogeneous solutions together with the corresponding homogeneous solution obtained for (1) the effective permeability calculated by *Gelhar and Axness* (1983) and the local dispersivity coefficients; (2) the equivalent permeability computed for each realization and local dispersivity coefficients and (3) equivalent permeability and effective dispersion. The last homogeneous medium was only tested for the dispersive case.

The values of the effective horizontal and vertical permeability computed with the expression of *Gelhar and Axness* (1983) are comparable to the equivalent values obtained numerically, showing a large variability that is not restricted to the depicted simulations. This variability points out the lack of ergodicity in the simulations. In these cases, the application of the expression of *Gelhar and Axness* (1983) is not appropriate since a single value does not reproduce properly all the heterogeneous simulations.

The use of homogeneous media with equivalent permeabilities and local dispersivity coefficients provides nonuniform results. The fit is good for some realizations (K13 in Figures 3.14

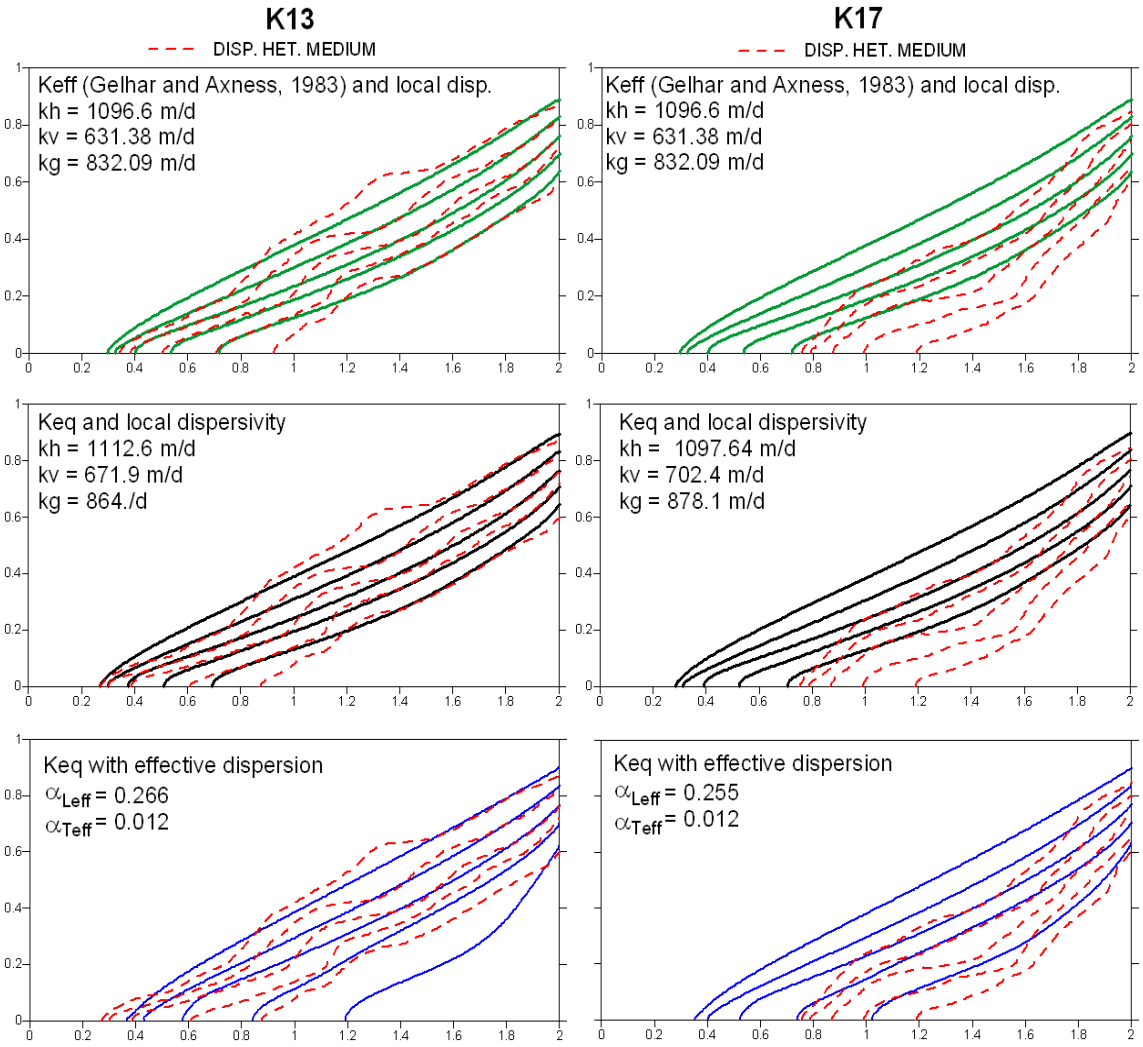

Figure 3.14: Dispersive solution of two heterogeneous realizations with medium λ and $\sigma^2 = 1$ (dashed lines) compared to the solution of three different homogeneous media. The parameters used are indicated in each case.

and 3.15), whereas the representation is poor for some others (K17), both in the dispersive and diffusive cases, as a result of the large fluctuation from realization to realization.

The effective dispersion does not offer satisfactory results either. The curve of Figure 3.3 provides large values of the effective longitudinal dispersivity coefficients. Therefore, the width of the mixing zone is overestimated at the bottom of the aquifer. However, the effective transverse dispersivity coefficients (Figure 3.3) have a small range of variation and are similar to the local

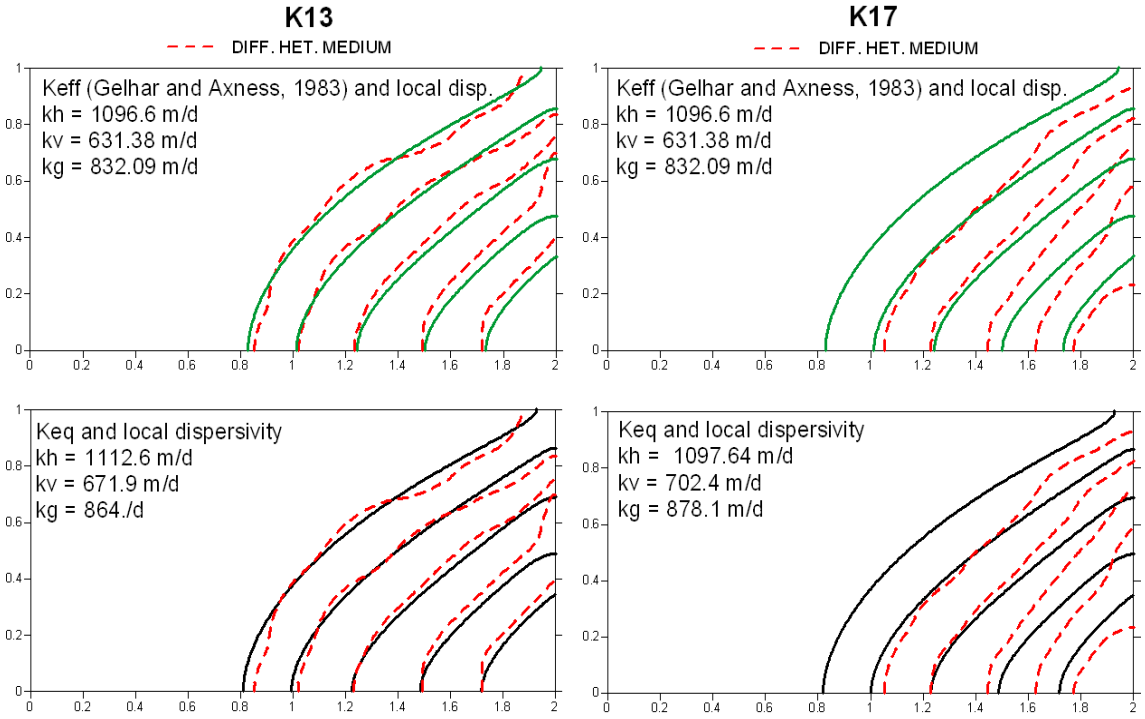

Figure 3.15: Diffusive solution of two heterogeneous realizations medium λ and $\sigma^2 = 1$ (dashed lines) compared to the solution of three different homogeneous media. The parameters used are indicated in each case.

dispersivity values. Therefore, the changes in the interface slope cannot be reproduced with these almost constant effective transverse values.

These results suggest that this type of heterogeneity cannot be reproduced by either local, equivalent or effective values. Medium scale heterogeneities should be explicitly represented to obtain satisfactory results in terms of the interface shape and location.

Ensemble

The ensemble of concentrations of the 50 heterogeneous simulations with medium λ and $\sigma^2 = 1$ is presented in Figure 3.16. The ensemble is compared with the solution of the homogeneous medium with (1) local dispersion/diffusion coefficients. For the dispersive case, Figure 3.17) shows the comparison with two homogeneous media; one with effective dispersion coefficients and

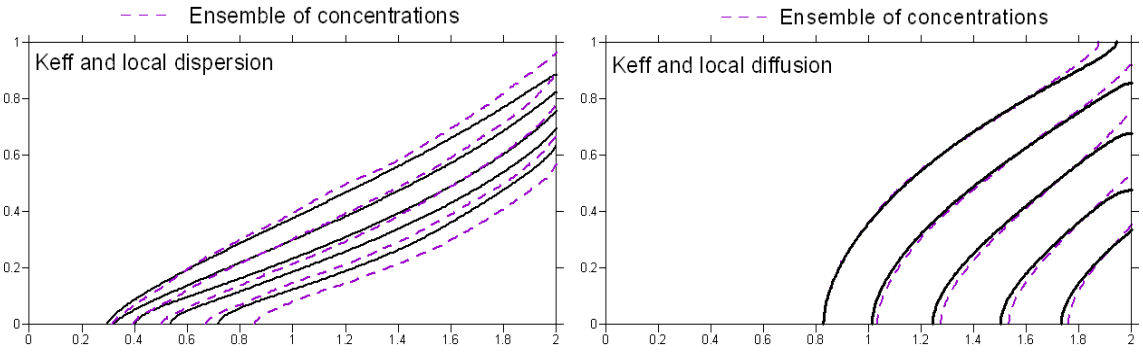

Figure 3.16: Ensemble of concentrations of the 50 heterogeneous realizations with medium λ and $\sigma^2 = 1$ (dashed lines) for the dispersive and diffusive case compared to the solution of a homogeneous medium with K_{eff} and local dispersion/diffusion

the other one with macrodispersion. In this case, none of them offer a satisfactory representation

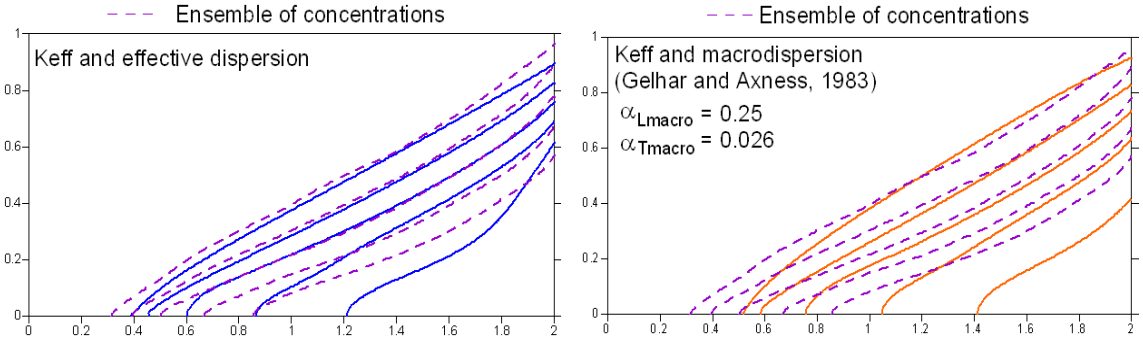

Figure 3.17: Ensemble of concentrations of the 50 heterogeneous realizations with short λ and $\sigma^2 = 1$ (dashed lines) for the dispersive case compared to the solution of a homogeneous medium with K_{eff} and (1) effective dispersion coefficients or (2) macrodispersion

of the mean behavior. The best approximation is obtained with the local dispersion coefficients. The effective dispersion coefficients overestimate the increase in the longitudinal dispersion while underestimates the increase in the transverse dispersion. However, the lack of ergodicity of these random realizations may cause the unsuitability of the efficient coefficients. The results obtained with macrodispersion show again that these values are not suitable for this study.

3.5.2 Large variance ($\sigma^2 = 2$)

Increasing the degree of heterogeneity, we considered a higher value of the permeability variance. Some of the heterogeneous results were presented in Figure 3.4 in Section 3. The dispersive interfaces show a large variability, not only in the toe location but also in the overall shape, resulting in convex and concave interfaces. A large variability in the toe position is also observed in the diffusive cases.

Effective parameters

The comparisons with the homogeneous media and the values of the effective and equivalent flow and transport parameters used are presented in Figure 3.19 and 3.18. The results are highly affected by heterogeneities and are, again, very different from one realization to another. These changes cannot be reproduced with any of the tested homogeneous media. In the cases in which better representations are obtained, the best fits are achieved with the equivalent permeability with local dispersion.

Effective dispersion values presented the same restrictions as in the case with smaller variance. The width of the mixing zone at the bottom is largely overestimated.

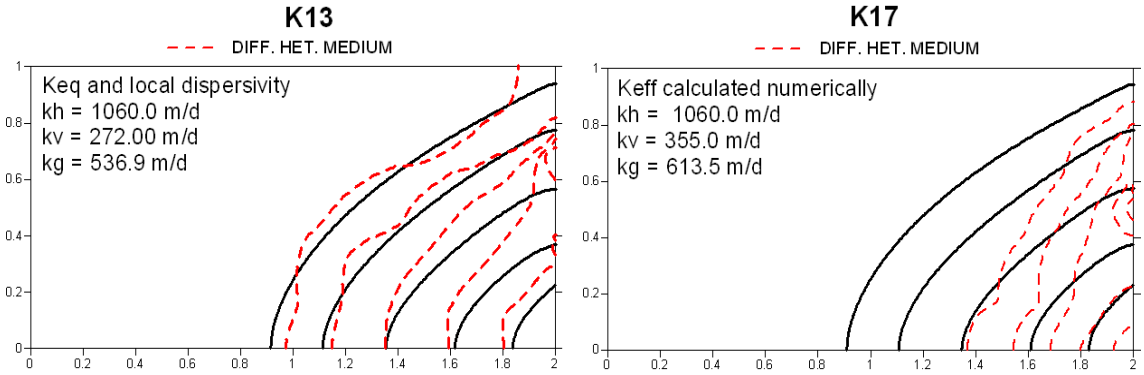

Figure 3.18: Diffusive interface (dashed lines) for two heterogeneous realizations (medium λ and $\sigma^2 = 2$) compared to an homogenous medium with the local diffusion coefficient.

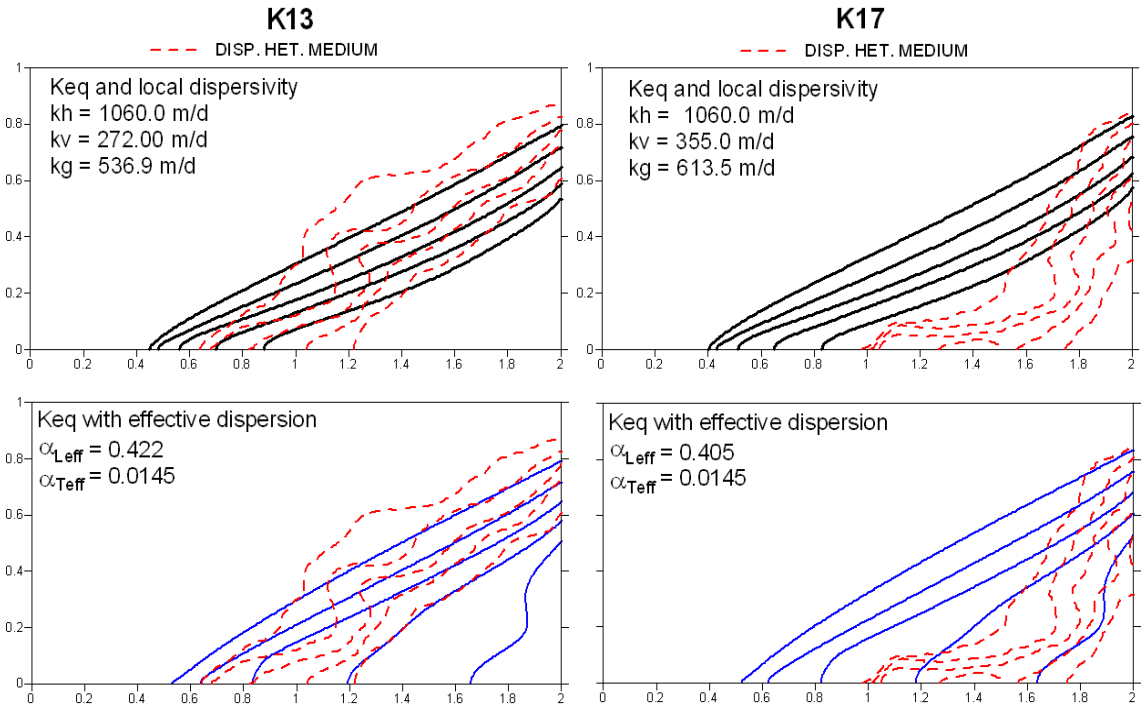

Figure 3.19: Isoconcentration lines for two heterogeneous realizations with medium λ and $\sigma^2 = 2$ (dashed lines) compared to a medium two homogeneous medium, one with local and the other with effective dispersivity coefficients.

3.6 Effects on characteristic output variables

We look at the variables of interest we defined in the methodological section in order to evaluate the effect of the increasing variance. We take into account the 50 realizations of each series and represent the distribution of their results in box-plots (Figure 3.20). The distribution of the heterogeneous media are compared to that of the media with equivalent permeability and local dispersivity values. The ensemble of the concentration of the heterogeneous fields is indicated with a rhomb.

The results show that:

- As explained above, heterogeneity produces a seaward movement of the toe location along with a widening of the mixing zone.

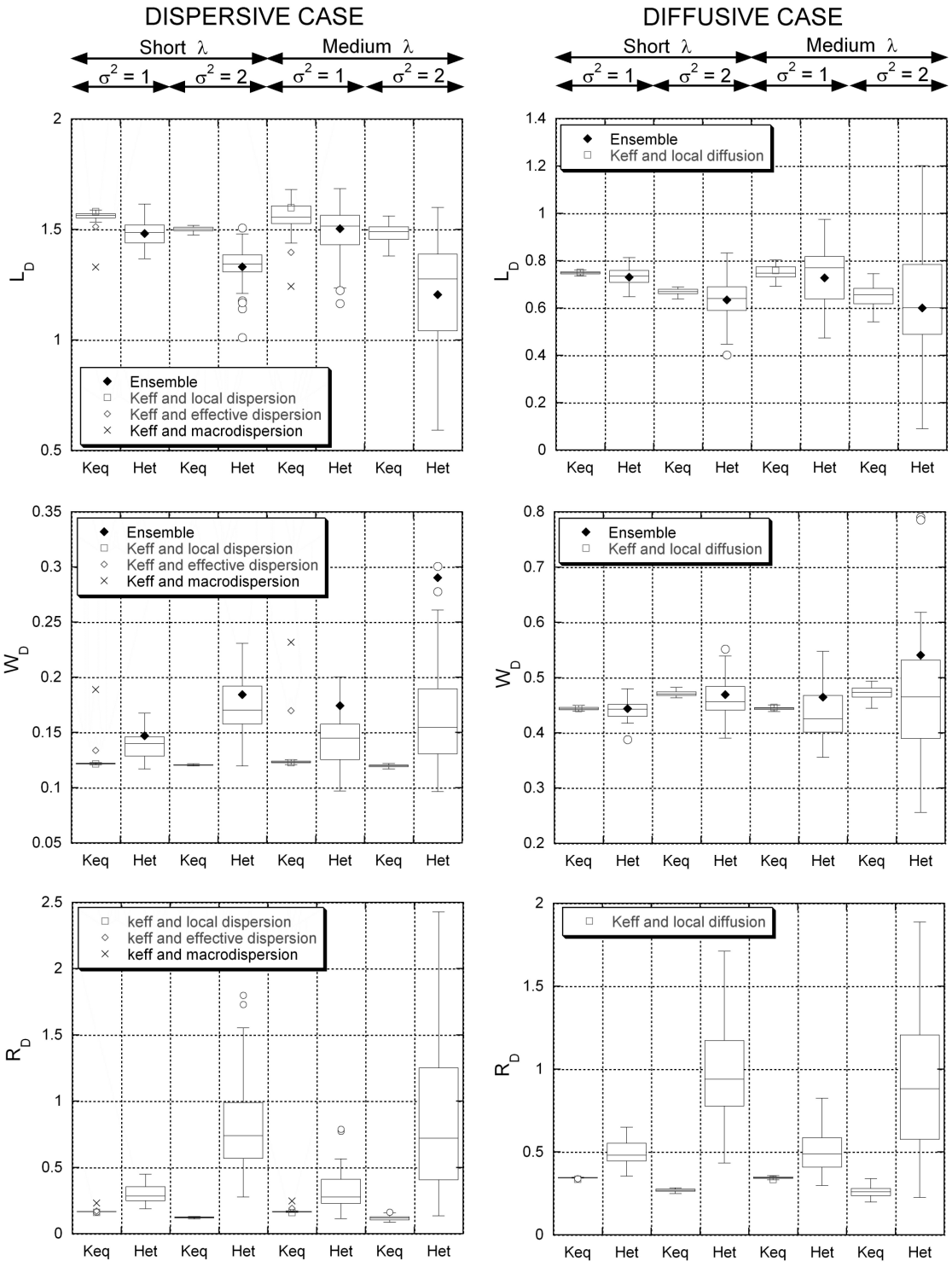

Figure 3.20: Box-plots showing the distribution of the results of L_D, W_D and R_D for the 50 random realizations of each series, their homogeneous media and the ensemble average of concentrations

- Increasing the variance causes a larger divergence between the heterogeneous and the homogenous media. L_D recedes further seawards and the width of the mixing zone becomes more irregular.

- Even though diffusive results show a larger variability of L_D and W_D than the dispersive case, the mean value of the heterogeneous results is closer to the homogeneous results than in the dispersive case, probably because of the higher diffusion value used in this type of problem (as discussed in previous chapter)

- The diffusive case with $\sigma^2 = 1$ is the only case in which the equivalent medium with local dispersion serves as a good representation of the heterogeneous simulations. This case coincides with the one studied by *Held et al.* (2005) and agrees with their result that the local diffusion was the appropriate representative transport parameter in this particular case.

The saltwater flux that enters the aquifer, R_D in Figure 3.20, increases with increasing heterogeneity. Increasing the degree of heterogeneity (i.e., increasing the variance) also increases the width of the distribution of R_D results. However, the distribution is comparable for the diffusive and dispersive cases, indicating that R_D is controlled by the particular permeability distribution (i.e., the realization) rather than by the diffusion or dispersion parameters.

As has been shown in the above presented results, the larger the variance, the larger is the variability in the slope of the dispersive interface, indicating a high variability in dispersion coefficients, in particular in the transverse dispersion coefficient. This variability is due to the large variability in the velocity fields.

Figure 3.20 allows us to compare the heterogeneous results with common σ^2 values to evaluate the effect of the correlation length. It is observed that, in general, large correlation lengths result in a wider distribution of the results due to the lack of ergodicity. For the same reason, the ensemble of the concentration is displaced with respect to the median of the distribution.

Except for the case of L_D for variograms with $\sigma^2 = 2$, the position of the median of the results

is not affected by the scale of the heterogeneity (i.e., λ). In general, the observed effect of the correlation length is negligible. This result is supported by the comparisons of the ensembles. Figure 3.21 compares ensembles for short and medium correlation lengths for the case of $\sigma^2 = 1$ (dispersive and diffusive cases). The superposition of both ensembles shows minimum discrepancies, revealing that the mean behavior is not sensitive to changes in the correlation length.

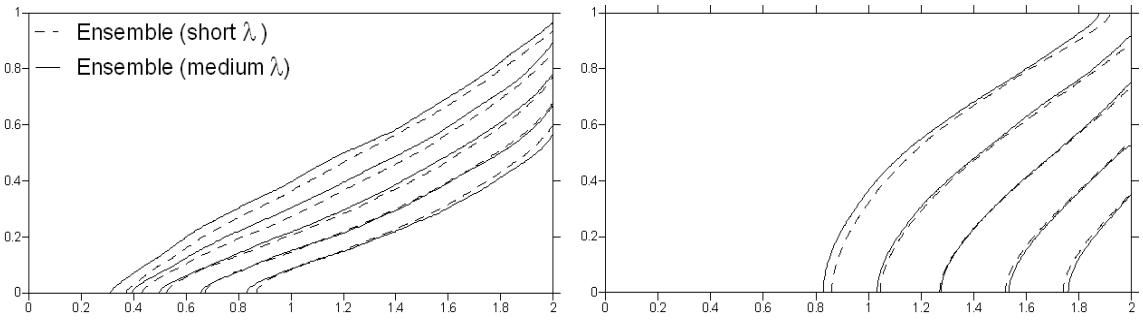

Figure 3.21: Comparison of the ensembles of the heterogeneous media with small correlation length (dashed lines) and with medium correlation length (solid line).

3.7 Discussion and conclusions

We have studied the effect of heterogeneity on seawater intrusion by considering two types of heterogeneity scales and two $ln(k)$ variances. We have described the results of single realizations and the mean behavior by computing the ensemble of the concentrations (for $\sigma^2 = 1$).

Qualitatively, heterogeneity causes the toe of the interface to recede while increases both the width and slope of the mixing zone. These displacements result in the rotation of the interface. In general, the shape of the interface and the saltwater flux depend on the distribution of the permeability in each realization. The latter is highly dependent on the permeability distribution near the seaside boundary. The interface slope is low in high permeability zones and high in low permeability zones. Freshwater channeling takes place in the high permeability zones resulting in an accommodation of the interface under high permeability zones. However, high permeability zones well connected to the seawater boundary result in preferential paths for incoming seawater.

Small convection cells are formed if these preferential paths are not well connected to other high permeability zones, but the overall aspect of the interface is not affected.

The large variability observed in R_D results suggest that this variable largely depends on the permeability distribution near the seaside boundary. Therefore, it is impossible to reproduce the results of this variable with representative homogeneous parameters. However, the toe penetration and the width of the mixing zone do not show large fluctuations, suggesting that they are susceptible of being reproduced by an homogeneous medium. The results of some realizations have been compared to different homogeneous media to evaluate in which case we can represent the heterogeneous media with effective parameters. Three homogeneous media have been contemplated:

- (KEFDL) An medium with the anisotropic effective permeability computed by means of *Gelhar and Axness* (1983) and local dispersivity/diffusion coefficients.
- (KEQDL) An medium with the equivalent anisotropic permeability tensor computed numerically for each single realization and local dispersivity/diffusion coefficients.
- (KEQDE) An medium with the equivalent anisotropic permeability tensor computed numerically and effective dispersivity coefficients (only for the dispersive case) obtained by the perturbation theory.

We find that for small correlation lengths and $\sigma^2 = 1$, both KEFDL and KEQDL provide a satisfactory representation of the heterogeneous diffusive results. These results agree with that of *Held et al.* (2005).

In the dispersive case, although these media provide good results, better ones are obtained with the implementation of effective dispersion coefficients (KEQDE), even though this case in the limit of application of the perturbation theory. Despite this good representation, dispersive results from all the considered variograms consistently reflect that the effect of heterogeneity induces a rotation of the interface. This rotation could be explained by an increase in the dispersion coefficients,

particularly in the transverse dispersion. The perturbation theory mainly increases the longitudinal dispersivity whereas the transverse dispersion remains close to its local value. Therefore, this rotation could not be reproduces with our effective values.

For larger values of the variance and the correlation length, neither of the homogeneous media provides a good representation of every single realization. However, for the ensemble of the large scale heterogeneity and $\sigma^2 = 1$, is again well reproduced by KEQDE.

Analyzing the separated effect of the correlation distance and the variance, results show that the critical factor is the variance whereas the mean value of toe penetration and the width of the mixing zone are not affected by changes in the correlation length.

Chapter 4

Quasi-horizontal circulation cells in seawater intrusion*

What makes saltwater intrusion different and more complex than other solute transport problems is that variation of concentration causes water density to vary in space and time. Density differences cause freshwater to float over seawater. This effect was first addressed by *Ghyben* (1889) and *Herzberg* (1901) who empirically found that the depth to saltwater correlates with freshwater head. Assuming equilibrium between the two fluids and that saltwater remains static, the depth of the freshwater/saltwater interface, z, is $\alpha_s z = h$; where h is the freshwater head, $\alpha_s = (\rho_s - \rho_f)/\rho_f$ where ρ_s and ρ_f are the seawater and freshwater densities, respectively. This is called the Ghyben-Herzberg approximation for seawater intrusion. Since α_s is approximately equal to 1/40, a frequent rule-of-thumb is to assume that the depth to seawater below sea level is 40 times the freshwater head above sea level.

A second effect associated with concentration differences is the mixing between the two fluids. Mixing is caused by diffusion/dispersion processes and results in some of the salt to be driven

*This chapter is based on the paper: Abarca, E., Carrera, J., Sanchez-Vila, X. and Voss, C.I., submitted for USGS approval. Quasi-horizontal convection cells in seawater intrusion

seawards by freshwater. Replenishment of this salt requires an inland flow of seawater. The result is a vertical convection cell formed by seawater that flows landwards at depth and disperses into the freshwater flowing zone, where salt is flushed out by the discharging freshwater flow (Figure 4.1). The equilibrium assumption of Ghyben-Herzberg is not valid because seawater flux causes an energy (head) loss. Therefore, the depth of the seawater wedge is underestimated. The above discussion indicates that seawater movement in coastal aquifers is caused by the combination of density driven flow and hydrodynamic dispersion. This effect was first discussed by *Cooper* (1964). When taking into account density effects, the groundwater flow and solute transport are coupled by the presence of the density in the gravity (buoyancy) term in the momentum balance equation of fluid.

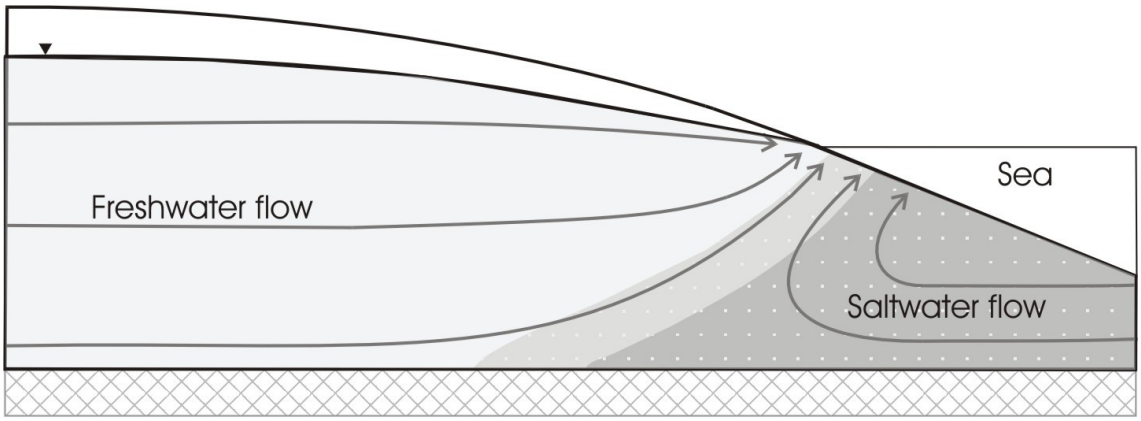

Figure 4.1: Classical vertical saltwater circulation cell induced by the combination of buoyancy forces and hydrodynamic dispersion processes.

Three-dimensionality may be a critical factor that has often been ignored when analyzing seawater intrusion processes. Irregular patterns of salinity be caused by many factors such as variable thickness formations , heterogeneity and variations in the depth of the aquifer boundaries, among others. The latter is the object of the present work. In homogeneous aquifers where the horizontal extent is large compared to the constant thickness, aquifer topography may become critical. The impact of gravity is given, in these cases, by the effective gravity, i.e., the projection of the gravity vector on the boundary planes. The effective gravity is controlled by the boundaries

slope and shape. When the lateral slope is large vertical flow can become of lesser order compared to the lateral flow.

Some geophysical studies provide evidence that seawater penetrates further inland at the deepest portion of coastal aquifers. *Flores-Márquez et al.* (1998) and more recently *Rangel-Medina et al.* (2003) compared the three-dimensional shape of the basement of the Costa de Hermosillo aquifer (Mexico) with geochemical and geophysical data. The crystalline basement presents a structure of alternating horsts and grabens and the integration of all available data indicates that preferential pathways for seawater intrusion correspond to the lineation of basement depressions (grabens). Yet, only two-dimensional density dependent flow cross sections of the aquifer were modelled. Thus, the three dimensionality of the flux due to the irregularity of aquifer bottom was not considered. *Benkabbour et al.* (2004) determined, by the Direct Current method, the depth of the bottom of the coastal aquifer of Mamora Plain, Morocco and the lateral and vertical distribution of salinity. Seawater penetrates further inland in the area of the Sebou River, where the substratum is deeper. This fact was attributed to the higher thickness and the proportionality of the seawater penetration with the square of the aquifer thickness inferred from Ghyben-Herzberg approximation. However, this assumption assumes that the total freshwater flow in each vertical section is constant. Buoyancy effects due to density differences were not taken into account.

The hydrogeological literature contains no qualitative analysis of the effect of aquifer morphology on seawater intrusion, although its importance has been considered in several heat transport studies. In those studies, variable density is taken into account and the effect of aquifer slope in the heat plume movement and velocity is addressed. *Bachu* (1995); *Bachu and Karsten* (2002) studied density driven flow in sloping aquifers, applying results to two sedimentary basins: Alberta (Canada) and Los Llanos (Colombia). *Malkovsky et al.* (2002) showed the importance of natural convection in a heat-generating liquid waste plume in a sloping aquifer, which could cause acceleration as well as slowing down of the plume depending on the system parameters. The role of aquifer's slope has also been addressed in brine movement in continental basins. a *Lahm et al.*

(1998) studied the role of salinity, derived variable, density flow in the displacement of brine from a shallow, regionally extensive aquifer and argued that density dependent flow causes a decrease in groundwater velocities and a reorientation of local flow directions of the aquifer within the mixing zone, but their model was 2D. *Assouline and Shavit* (2004) studied the effects of management policies, including artificial recharge, on salinization in a sloping aquifer in Israel. Although seawater intrusion processes were not taken into account, the importance of the thickness variations in the sloping aquifer in the salinization process was addressed.

Three-dimensional modeling of density dependent flow and solute transport is a useful tool to assess the effect of aquifer morphology in seawater intrusion. Until recently, 3D models were not practical due to high computer time requirements. As a result, most seawater modeling studies consisted of 2D cross section models or sharp interface models. However, three-dimensional density dependent flow models have been developed in the last decade, resulting in better ways to model advective and dispersive mechanisms with fluid density and viscosity effects. Nowadays, many codes are available: FEFLOW (*Diersch and Kolditz*, 1998), ROCKFLOW (*Kolditz et al.*, 1998), HST3D (*Kipp*, 1986), TVDT3D (*Ackerer et al.*, 1999), METROPOL (*Sauter et al.*, 1993), MVAEM (*Strack*, 1995), MOCDENSE3D (*Oude Essink*, 1998), SWICHA (*Huyakorn et al.*, 1987), SWIFT (*Ward*, 1991), CODESA (*Gambolati and Paniconi*, 1999), SUTRA (*Voss and Provost*, 2002), SEAWAT (*Guo and Langevin*, 2002) and d^3f (*Fein and Schneider*, 1999). A recent 'state-of-the-art' of density-dependent flow modelling in porous media can be found in *Diersch and Kolditz* (2002). Improvements in computer speed make increasingly feasible to build sufficiently refined grids to reduce problems of numerical dispersion, which explains the emergence of 3D benchmark problems (*Johannsen et al.*, 2002; *Oswald and Kinzelbach*, 2004) for density dependent codes. Variable density 3D models of real cases are also becoming increasingly frequent (*Oude Essink*, 2001; *Xue et al.*, 1995; *Barrocu et al.*, 1994; *Gambolati and Paniconi*, 1999; *Bear et al.*, 2001; *Paniconi et al.*, 2001a; *Gingerich and Voss*, 2002; *Milnes and Renard*, 2004). Complex geometries are included in these real cases but no reference to the effect of the boundaries shape is made in the analysis of the results, either because it is not remarkable or

because it has not been considered.

In summary, emphasis has been never been placed on analyzing the effect of aquifer topography on seawater intrusion, particularly the effect of lateral variations in aquifer depth. The objective of this paper is precisely to test the conjecture that aquifer bottom topography may significantly affect seawater intrusion patterns in coastal aquifers. First, the governing equations and some dimensionless numbers that can be used to characterize the effects upon groundwater flow patterns of aquifer bottom topography are presented. Then, a suite of numerical simulations including a sensitivity analysis is used to show the potential importance of this phenomenon in real coastal aquifers.

4.1 Governing equations and dimensionless numbers

Modelling seawater intrusion requires simulating the flow of variable density water and the transport of salt. These two equations are coupled through water density, which enters in the flow equation and is a function of concentration. The result is a set of two coupled non-linear equations. Nonlinearity further causes the density dependent flow to be very sensitive boundary conditions and variability in the permeability field. Nonlinearity causes fingering and rotational flow with closed streamlines when the initial configuration of the system is not stable. This call for a proper description of the 3D problem. Equations governing these phenomena are presented in this section.

4.1.1 Flow equation

Flow of any fluid is governed by mass and momentum conservation. Mass conservation can be written as:

$$\frac{\partial \rho \phi}{\partial t} = -\boldsymbol{\nabla} (\rho \boldsymbol{q}) + \rho^* Q_h \tag{4.1}$$

where ρ is the fluid density (kg/m^3), ϕ is porosity (volume of voids per unit volume of aquifer), $\boldsymbol{q}$ is fluid flux ($m^3/s/m^2$), and Q_h is the sink/source term (m^3/s of fluid per unit volume of aquifer), ρ^* is the density of the incoming water through the source terms.

Dependence of density on solute mass fraction is frequently described by a linear or an exponential law (*Kolditz et al.*, 1998). A linear equation would read:

$$\rho(\omega) = \rho_f + \beta_\omega \left(\omega - \omega_f\right) \tag{4.2}$$

where ω is the solute mass fraction (kg of salt/kg of fluid), β_ω is the constant relation between the density and the salt mass fraction variation, ω_f is the freshwater salt mass fraction and ρ_f is the density of freshwater.

The flow equation can be written in terms of either pressure p (Pa) or equivalent freshwater head h_f (m). The freshwater equivalent head is defined as:

$$h_f = \frac{p}{\rho_f g} + z \tag{4.3}$$

Momentum conservation in flow through porous media is expressed by Darcy's law

$$\boldsymbol{q} = -\frac{\boldsymbol{k}\rho_f g}{\mu}\left[\boldsymbol{\nabla} h_f + \alpha \boldsymbol{\nabla} z\right] \tag{4.4}$$

where $\boldsymbol{k}$ is the intrinsic permeability tensor (m^2), μ is the fluid viscosity (kg/ms), $\alpha = \rho - \rho_f/\rho_f$ and $\boldsymbol{\nabla} z$, in 3D, represents a unit vector opposite to gravity. This explains why the second term in 4.4 represents buoyancy. In relatively thin aquifers, where flow is confined to take place within the aquifer plane, $\boldsymbol{\nabla} z$ can be approximated by the aquifer slope. It is common to write (4.4) in terms of the hydraulic conductivity of freshwater $\boldsymbol{K} = \boldsymbol{k}\rho_f g/\mu$.

Finally, expanding (4.1) and using (4.4), the mass balance equation for general saturated prob-

lems is:

$$\rho S_s \frac{\partial h_f}{\partial t} + \rho\phi\beta_\omega \frac{\partial \omega}{\partial t} - \boldsymbol{\nabla}\Big(\boldsymbol{K}\big(\boldsymbol{\nabla} h_f + \alpha \boldsymbol{\nabla} z\big)\Big) - \rho^* Q_h = 0 \tag{4.5}$$

where S_s is the specific storage coefficient.

4.1.2 Transport equation

The mass balance of solutes is expressed in terms of solute mass fluxes, $\boldsymbol{j}$ (advective, diffusive and dispersive), as:

$$\frac{\partial (\rho\phi\omega)}{\partial t} = -\boldsymbol{\nabla}\left(\boldsymbol{j}_{adv} + \boldsymbol{j}_{diff}\right) + \rho^* Q_h \omega^* \tag{4.6}$$

The advective mass flux is equal to $\boldsymbol{j}_{adv} = \rho \boldsymbol{q} \omega$. The dispersive and diffusive fluxes are treated together as $\boldsymbol{j}_{diff} = -\rho \boldsymbol{D} \boldsymbol{\nabla} \omega$ where $\boldsymbol{D}$ is the hydrodynamic dispersion tensor.

4.1.3 Dimensionless Numbers

The motivation of this analysis comes from Darcy's law expressed in equivalent freshwater head (4.4). The first term is essentially directed towards the sea in unpumped aquifers. However, in aquifers with irregular bottoms, the second term may not. In fact, if the aquifer's slope is large, this term may become prevalent. For example, if $\alpha_s = 1/40$ and the aquifer slope, $\partial z/\partial y = 4\%$ (y being the coordinate parallel to the coast), then the second term becomes 0.1%, which is a sizable value in comparison with $\boldsymbol{\nabla} h_f$. In such a case, buoyancy would cause a lateral flux, leading to the development of a lateral convection cell.

In order to analyze the effect of aquifer bottom topography, two dimensionless numbers are defined. The first one, N_b, is defined by comparing the two terms in equation (4.4). The first term, the freshwater head driven flow ($\boldsymbol{K}\boldsymbol{\nabla} h_f$), is approximated by the boundary freshwater influx, q_b. In

the second one (buoyancy term), the gradient of altitude is approximated by the maximum slope of the aquifer bottom, m; this is applicable when the aquifer thickness is small compared to horizontal extent. Therefore, an "aquifer bottom buoyancy" dimensionless number may be defined:

$$N_b = \frac{\alpha_s / \boldsymbol{K}\boldsymbol{\nabla} z /}{/\boldsymbol{K}\boldsymbol{\nabla} h_f /} \approx \frac{\alpha_s / \boldsymbol{K} m /}{q_b} \tag{4.7}$$

However, for the purposes of this work it is more appropriate to consider a "lateral buoyancy" dimensionless number, N_{by}, by comparing the seawards driving force to the lateral component of buoyancy (y coordinate, parallel to coast):

$$N_{by} = \frac{\alpha \boldsymbol{K} \partial z / \partial y}{q_b} \tag{4.8}$$

The dimensionless number defined in (4.7) resembles the Driving Forces Ratio (DFR) proposed by *Bachu* (1995) and *Bear* (1972) to define free and forced convection in vertical flow.

$$DFR = \frac{\alpha}{\boldsymbol{\nabla} h_f} \tag{4.9}$$

The numbers defined here, N_b and N_{by}, are preferable to DFR, because the fresh water flux is usually better defined than $\boldsymbol{\nabla} h_f$. Moreover, these numbers explicitly take into account the aquifer slope, which induces an important driving force in geometrically confined aquifers. This has been recognized by *Dorgarten and Tsang* (1991) who proposed an expression for DFR essentially identical to (4.7), although motivated by heat transport. Yet, N_{by} is preferred because it is the lateral slope ($\partial z / \partial y$) that causes flow to depart from the vertical plane.

4.2 Numerical modelling methodology

A numerical methodology is employed to evaluate the extent to which aquifer depth variation can contribute to irregularities in saltwater intrusion patterns. A 3D model of a confined aquifer of constant thickness is considered. An aquifer size of 10000 x 5000 x 50 m^3 is chosen resembling typical dimensions of coastal aquifers. In order to save computation time, the numerical analysis was carried out modelling only half of the symmetric aquifer (see Figure 4.2).

Several aquifer geometries of a horizontally large confined aquifer of constant thickness, as presented in Figure 4.3, were studied. They can be grouped into four cases: (1) "horizontal", (2) "sloping" (towards the sea), (3) "V-shaped" (with a central deeper section) and (4) a "warped" aquifer (curved with a deeper point located in the middle of the seaside boundary). All geometries are symmetric, in order to take advantage of the numerical simplification described in Figure 4.2.

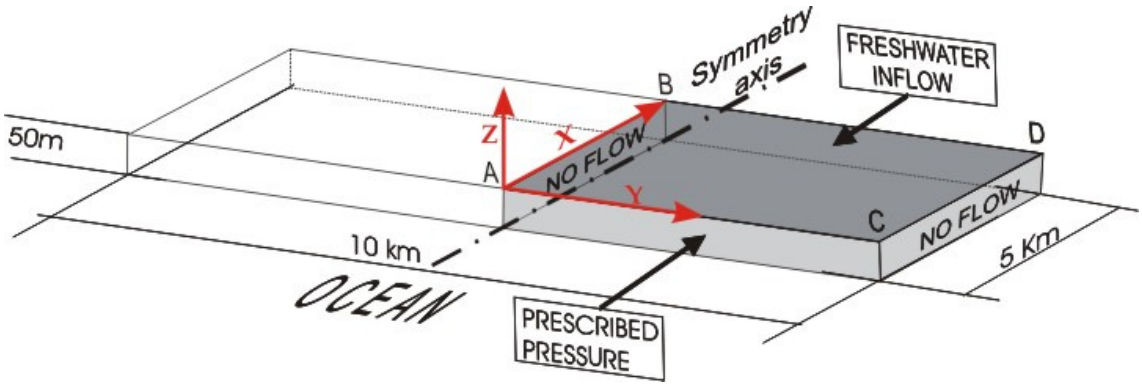

Figure 4.2: Geometry of the aquifer and model domain (grey area), including boundary conditions: freshwater inflow inland and specified pressure in the seaside boundary.

Boundary conditions used are:

1. Constant freshwater ($\omega = 0$) inflow from inland (1.18 $hm^3/year$ across the whole boundary) at the vertical BD section in Figure 4.2.

2. Specified pressure along the seaside boundary ($p = \rho_s g z$) with solute concentration equal

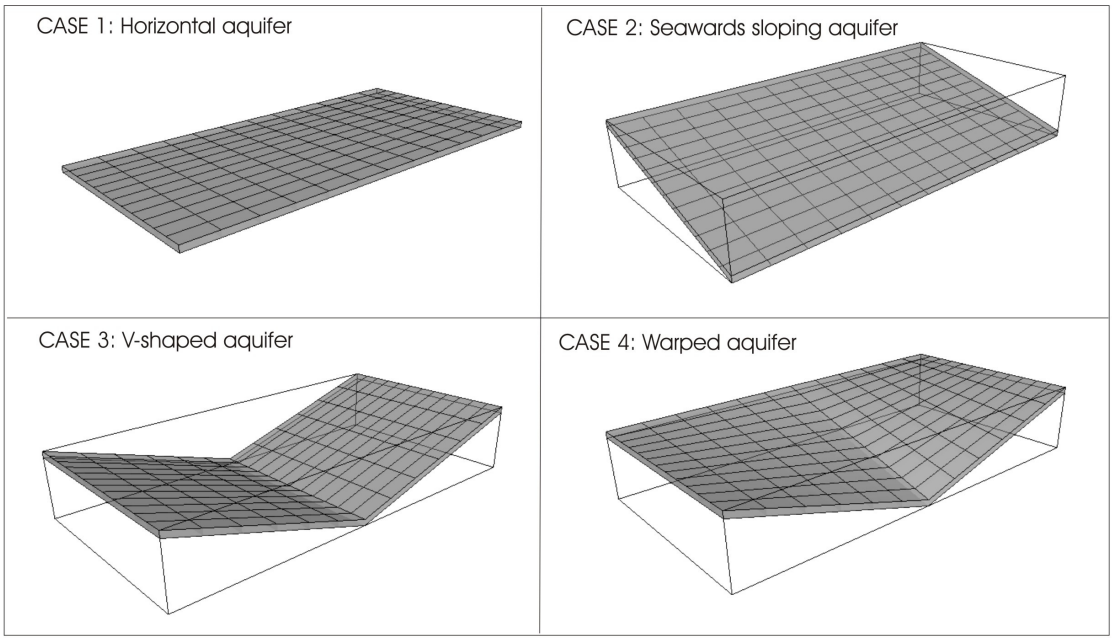

Figure 4.3: Schematic description of the test cases geometries: (1) horizontal, (2) seawards sloping, (3) V-shaped and (4) warped. Freshwater flows from the background (inland) towards the foreground (seaside).

to seawater concentration for inflowing portions and resident concentration for outflowing boundaries at the vertical plane passing through AC in Figure 4.2.

3. The remaining boundaries (vertical planes passing through AB and CD in Figure 4.2 and top and bottom surfaces) are closed to flow and solute transport.

Both sea level and the horizontal plane (ABCD in Figure 4.2) are set at $z = 0$. Flow and transport parameters used for the simulation are specified in Table 4.1. The simulated cases are depicted according to the boundary planes' shape and slope and the N_{by} parameters in Table 4.2. The lateral slopes chosen for the test cases are 1%, 3% and 10%. Therefore, there are three simulations with N_{by} = 0.2, 0.6 and 2.04, respectively.

Table 4.1: Parameters used in the simulations

Parameter	Value	
ϕ	0.2	Porosity
k	1.25e-11 m^2	[1]Permeability (isotropic)
$\alpha_{Lmax} = \alpha_{Lmed}$	20 m	Max. and med. longitudinal dispersivity
α_{Lmin}	2 m	Min. longitudinal dispersivity
α_T	2 m	Transverse dispersivity
D_m	1.0e-9 m^2/s	Molecular diffusion coefficient
α	1.0e-8 $(kg/ms^2)^{-1}$	Matrix compressibility
β	4.4e-10 $(kg/ms^2)^{-1}$	Fluid compressibility
μ	0.001 g/ms	Freshwater viscosity

[1] *This permeability is equivalent to a freshwater hydraulic conductivity of 1.225e-4 m/s*

Table 4.2: Description of simulations considered in the analysis (m_x and m_y are the components of the slope perpendicular and parallel to the sea coast, respectively)

Test case	Max m_x	Max m_y	N_{by}
1: Horizontal	0	0	0
2: Seawards sloping	0.01	0	0
2: Seawards sloping	0.03	0	0
2: Seawards sloping	0.1	0	0
3: V-shaped	0	0.01	0.2
3: V-shaped	0	0.03	0.6
3: V-shaped	0	0.1	2.04
4: Warped	0.01	0.01	0.2
4: Warped	0.03	0.03	0.6
4: Warped	0.1	0.1	2.0

Computer simulations were performed with SUTRA (*Voss and Provost*, 2002). The numerical technique used is the Galerkin finite element method with hexahedral elements. Implicit finite differences are used for time integration. The iterative methods chosen to solve the linear system of equations are the conjugate gradient method for the flow equation and GMRES for the transport equation. The Picard method is used to solve to the non-linear system. The mesh consists of 36 x 73 x 11 nodes and 25200 hexahedral elements. A fine discretization in the vertical direction is required to achieve good resolution of the interface shape as well as to avoid numerical dispersion

in the vertical direction. Horizontal discretization is finer near the seaside boundary as well as in the boundary representing the symmetry axis (AB in Figure 4.2) with a resolution of 25 m.

Results are analyzed for natural steady state. The simulations are the result of a transient run of 1500 years, starting from the initial concentration and pressure conditions that describe a completely fresh-water aquifer. The steady-state position of the saltwater-freshwater interface is reached in all cases. Simulations with geometries without lateral slope need less than 100 years to reach steady-state. However, the required time increases when increasing N_{by} , needing as much as 1500 years for the simulations with largest N_{by} values.

The dispersion tensor used in the SUTRA code comes from an anisotropic-media dispersion model (*Voss and Provost*, 2002) that allows dispersion to vary depending on flow direction. This implementation is important to characterize transport in highly heterogeneous media, for instance, layered aquifers. Also large horizontal extent aquifers with reduced aquifer thickness need this kind of dispersion model to represent vertical transport (as in seawater intrusion process) because of the different scales in the horizontal and vertical directions.

4.3 Results

In order to compare similar values in all the simulations, the 50% isoline is selected as a representative value in the analysis of saline intrusion. A particular but most important point in this line is the ”toe” position, defined as the distance (measured along the x axis direction) between the seaside boundary and the point in which the 50% isoline intersects the aquifer bottom. Results are presented as a function of the slope (m_x or m_y) and they are compared to the horizontal aquifer results which are taken as a reference.

4.3.1 Aquifers without lateral slope

The interface positions for the horizontal (case 1) and seawards sloping (case 2) aquifers with 1, 3 and 10% slope are shown in Figure 4.4a. When the slope is directed towards the sea (Figure 4.4a), intrusion patterns are very similar to those of horizontal aquifers. In other words, the interface geometry is not significantly affected by this slope. As the slope increases, the interface is slightly displaced seawards. The toe is somewhat displaced seawards both because of the no flow (nor transport) bottom boundary condition and because although the interface shape is the same, as the slope increases, the intersection of the interface with the aquifer bottom occurs closer to the seaside boundary.

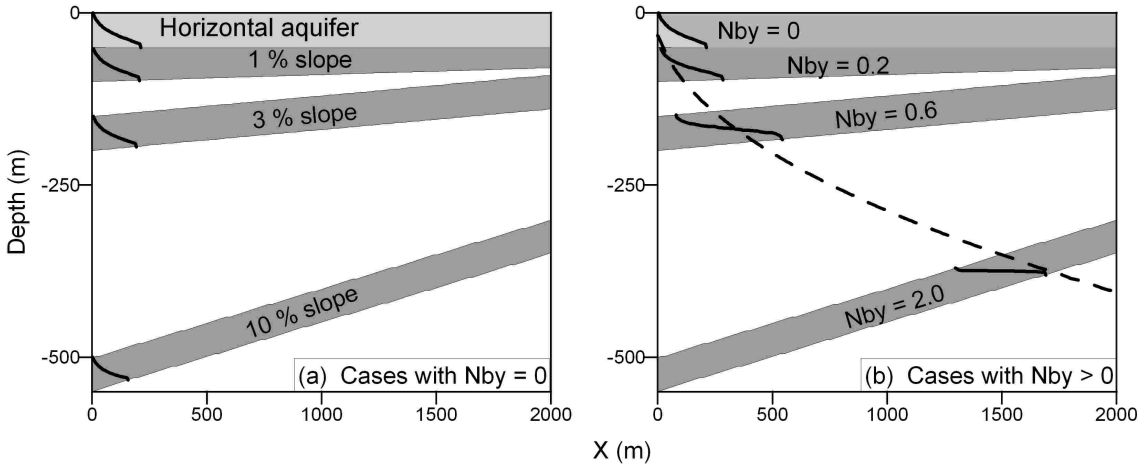

Figure 4.4: (a) Interface position in case 1 (horizontal) and 2 (seawards sloping) in the central cross section (vertical plane through BA in Figure 4.2); (b) Interface position in horizontal and warped aquifers. The dashed line represents the interface for a horizontal 550 m thick aquifer with the same inland unit flux. Horizontal axis is distance to the sea boundary (in meters); the vertical axis shows the depth (meters).

4.3.2 Lateral sloping aquifers

The saltwater intrusion pattern discussed above is strongly modified in aquifers with a nonzero lateral slope (N_{by} greater than 0). This is illustrated in Figure 4.4b which displays interface positions at a central cross section for warped aquifers with 1, 3 and 10% lateral slopes. It is clear that

increasing N_{by} value leads to a broader seawater penetration in the central section of the aquifer. It is interesting to notice that the interface for these aquifers coincides approximately with that of a horizontal 550 m thick aquifer with the same unit flux and dispersivity (dashed line in Figure 4.5b). This thickness (550 m) is the maximum difference in elevation between the top and the bottom boundaries of the warped aquifer with highest slope.

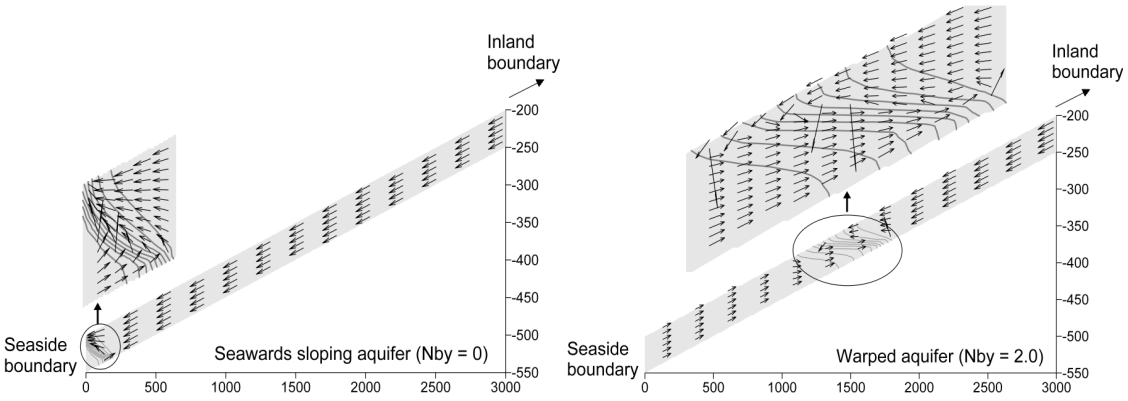

Figure 4.5: Velocity vectors on the aquifer central cross section (AB vertical section in Figure 4.2) projected in the XZ plane: (a) Cross section of a seawards sloping aquifer with a 10% slope. Notice the typical vertical convection cell, with seawater entering in the lowest part of the aquifer and exiting in the upper part. (b) Cross section of a warped aquifer with N_{by}=2.0. Notice that in this section, seawater enters through the whole aquifer thickness. Vector lengths indicate the magnitude of the velocity in each element.

Enhanced seawater intrusion in the deepest portion of the warped aquifer can be properly illustrated by comparing the velocity vectors in a seawards sloping aquifer and a warped aquifer with equal seawards slope at the central section. Velocity fields and interfaces for case 2 and 4 (both with m_x = 10%) in the central cross section of the aquifer are shown in Figure 4.5. Vectors show the expected local flow directions in the sloping aquifer (Fig. 4.5a). Freshwater discharges to the sea, and a vertical convective cell is formed by saltwater entering from the seaside. However, the interface is far from the sea boundary in the warped aquifer (Fig. 4.5b). There is no discharge of freshwater at the shown cross-section and the velocity vectors might suggest that seawater flows inland and mixes along the interface area with all the incoming freshwater. All the incoming seawater need a discharge zone that is not evident when looking at the velocity vectors in this

vertical section. This apparent unrealistic result becomes clear when the problem is analyzed in three dimensions. Figure 4.6 displays the velocity vector field, the isoconcentration lines and the equivalent freshwater head isolines on the aquifer bottom for the V-shaped and warped cases with N_{by} equal to 2.0. It is clear that the lateral slope causes the convection cell in the saltwater wedge to develop sideways. This explains why seawater entering the deepest portion of the aquifer penetrates so far inland. It also explains why seawater velocities are reduced near the interface in 4.5. Seawater is actually deflected sideways and upslope. The same happens to freshwater, which is pushed by the entering seawater and can only discharge in the shallower portions of the shore.

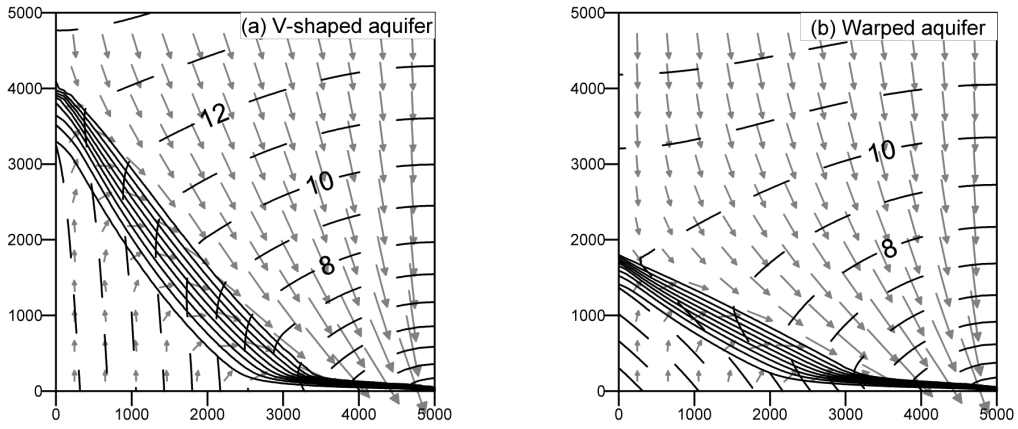

Figure 4.6: Velocity vectors at the aquifer bottom projected in the XY plane, isoconcentration lines and equivalent freshwater head isolines (dashed lines) in a V-shaped (a) and warped (b) aquifer with N_{by}=2.0. Notice that water entering the aquifer through its lowest point tends to exit at the much higher right hand corner, thus leading to an essentially horizontal convention cell. The lines (10% to 90% mixing lines) show the position and width of the mixing zone at the aquifer bottom. Notice that both fresh and salt waters are deflected sideways towards the high end of the outflowing boundary

Both saltwater penetration and interface shape are conditioned by the three dimensional pattern of the flow field. Therefore, a different penetration between the central and the seaside cross-sections are observed in all the examples considered with N_{by} different from 0. The relationship between seawater penetration (toe position) in a central cross section and N_{by} is represented in

Figure 4.7a for all simulated cases. Toe penetration increases significantly with the lateral slope at the aquifer central section (Figure 4.7a). This effect is accompanied by an opposite one in the shallowest end section (in this case the lateral boundary section, given by a vertical plane trough CD in Figure 4.2) as shown in Figure 4.7b. The interface penetration decreases in this section as the N_{by} number increases due to the higher amount of freshwater that is diverted to the shallowest portions of the aquifer.

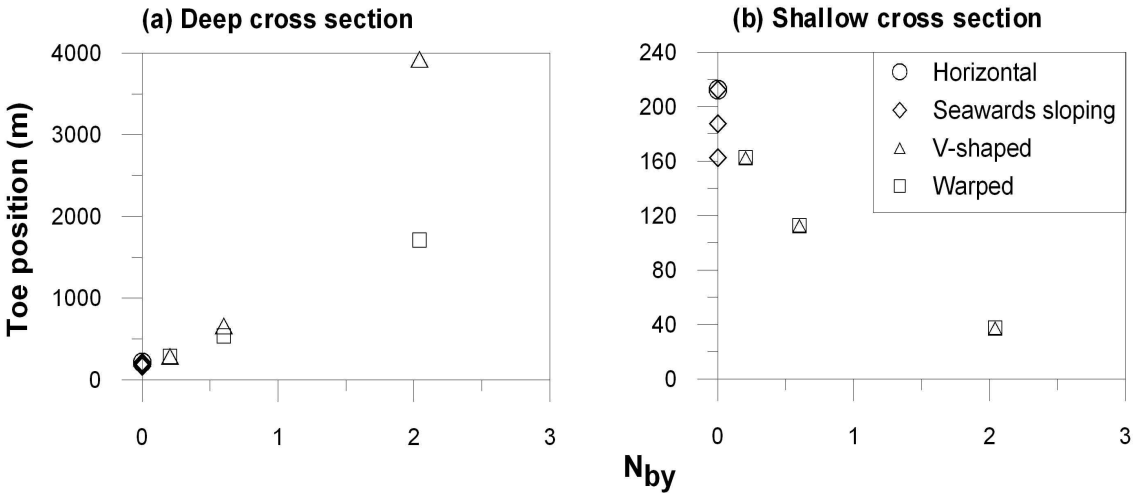

Figure 4.7: Toe position for the central cross section (a) and the lateral cross section (b). Notice the relation between the Nby number and the increase of the salt penetration in the central section. This effect is also accompanied by a decrease of toe penetration at the lateral boundary, which is caused by the convergence of freshwater outflow at the upslope portion of the aquifer.

As a consequence of the three-dimensionality of flow the salt mass flux that comes into the aquifer through the seaside boundary is not equally distributed along the coast for aquifers with a lateral slope as shown in Figure 4.8. Vertically integrated flow is virtually equal to 0 for aquifers without lateral slope as expected because of the symmetry of the flow field. Two zones can be distinguished along the coast line in warped and V shaped aquifers: an inflow and an outflow dominated zones. The maximum salt outflow value depends on the extent of the horizontal convection cell formed and observed in Figure 4.6, and therefore, on the N_{by} number. When N_{by} equals 2.0, salt enters the aquifer through the deepest half of the seaside boundary. Salt discharge takes place upslope, with a maximum about 3000 meters away from the central and deepest part of

the aquifer. These values become 500 m (salt inflow zone) and 900 m (maximum salt discharge) for N_{by} equal to 0.6.

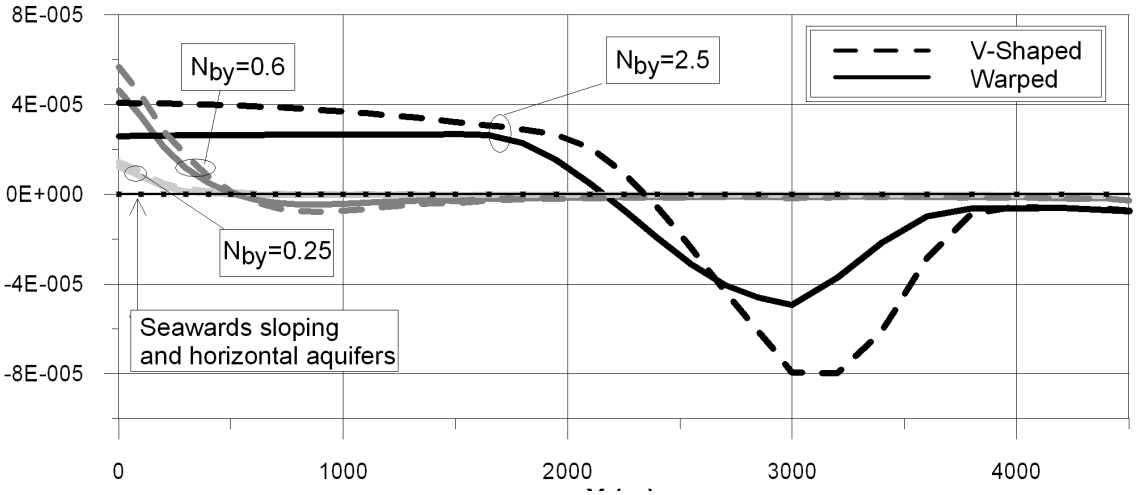

Figure 4.8: Vertically integrated salt flux per unit length of coastline. Positive values indicate salt inflow and negative values, outflow. The minimum salt flux in each case indicates the location of the main salt discharge point. Notice that the mass flux is 0 along the whole boundary in both horizontal and seawards dipping aquifers. However, seawater enters inland at the deepest portions of the aquifer and exits at shallower portions, though not at the shallowest, in aquifers with lateral slope

Three dimensionality of the flow also implies that the generally used estimation of the saltwater wedge toe position via the Ghyben-Herzberg approximation is not valid when the aquifer has a lateral slope. The assumption of constant horizontal freshwater flow perpendicular to the coast is not met. Still, in Appendix A, an approximation is derived for the case of laterally sloping aquifers based on the Ghyben-Herzberg assumptions (sharp interface and immobile saltwater). Figure 4.9 shows the comparison between the model results (50% mixing line) and the toe position calculated with the tilted Gyben-Herzberg approximation (Appendix A). Two different interface positions have been calculated. The first assuming that the interface intersects the coast line in the shallowest point, which is the standard in 2D vertical models and it is known to overestimate seawater penetration. The second one is based on supposing that the interface intersects the coast line at the main salt discharge point (Figure 4.8). The second approximation fits the model results

accurately, however, the main discharge point is not an easy parameter to know in advance. Toe penetration is slightly overestimated by the first approximation. Still, it can be considered as good approximation to the solution of the interface position as it is in vertical cross sections.

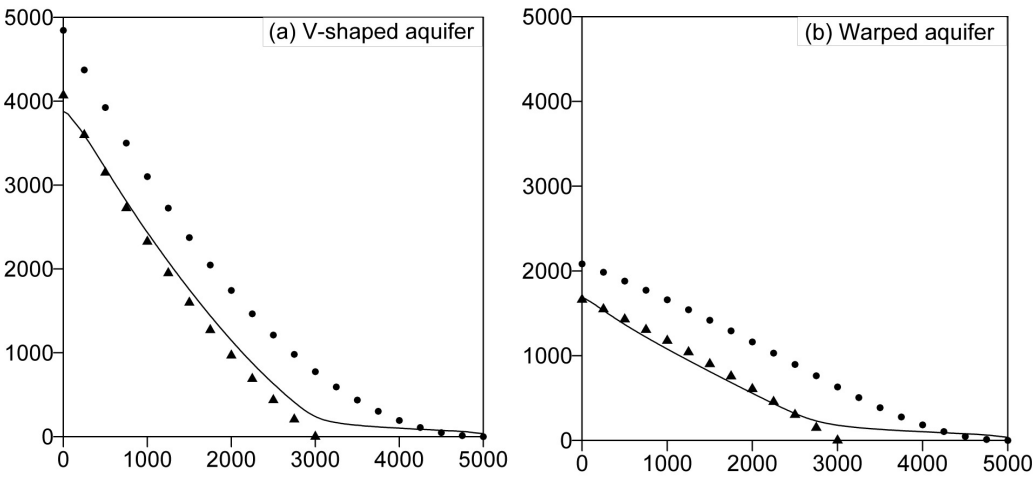

Figure 4.9: Model results (50% mixing is shown as a continuous line) at the bottom of the V-shaped (a) and warped (b) aquifers with $N_{by} = 2.0$. Also shown is the location (dots) of the interface derived from the Ghyben-Herzberg approximation of Appendix A for areal two dimensional aquifers with the same elevation. The tilted interface position calculated assuming that it intersects the coastline at the shallowest point is shown by circles. Triangles represent the solution assuming that the interface intersects the boundary at $y = 3000m$, the main salt discharge point as shown in Figure 4.8.

4.4 Sensitivity analysis

Other parameters may affect the behavior of saltwater intrusion in aquifers with variable depth. In order to determine whether this effect is well characterized by the N_{by} number, the sensitivity of toe position to dispersivity coefficients, freshwater incoming flux (q_b) and aquifer thickness (b) is studied.

4.4.1 Dispersivity

Results of the sensitivity analysis with respect to dispersivity are shown in Figure 4.10. As explained in previous sections, the dispersivity tensor used can deal with three different values of the longitudinal dispersion coefficient (α_L). α_L values are the same for horizontal flow directions but ten times larger than α_L for vertical flow. To simplify, the transverse dispersivity coefficient (α_T) is the same for all flow directions. The toe penetration in a central cross section shows the expected behavior. As dispersivity coefficients are increased, the toe penetration decreases. Toe penetration is more sensitive to transversal than to the longitudinal dispersivity. However, in both cases, sensitivity is low and does not affect the behavior discussed above.

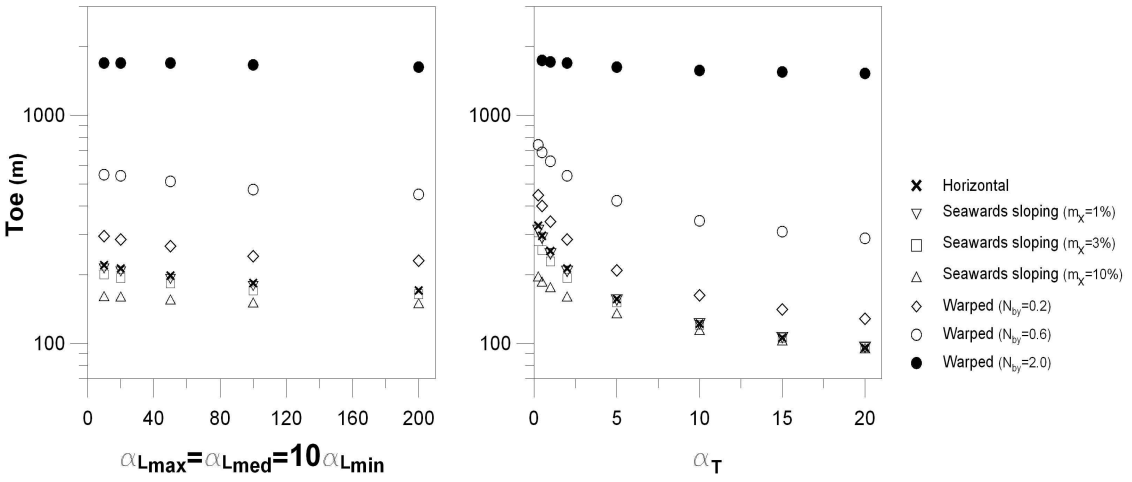

Figure 4.10: Sensitivity of toe penetration in the aquifer central cross section to the longitudinal (left) and transversal (right) dispersivity values for different aquifer geometries.

4.4.2 Freshwater boundary inflow

Freshwater inflow (q_b) is one of the parameters that appears in the N_{by} expression. Several simulations were carried out to assess the effect of this factor in the seawater intrusion behavior in lateral sloping aquifers. The toe positions obtained for different values of the freshwater inflow

are shown in Figure 4.11 for some of the geometries considered. The larger the freshwater inflow is, the smaller the saltwater penetration is. However the observed different behavior for the aquifers with $N_{by} > 0$ is still observed for higher values of the freshwater boundary inflow.

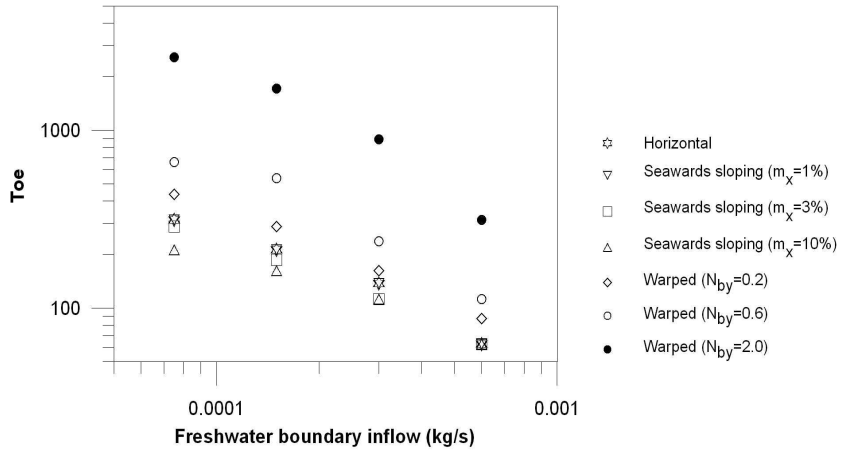

Figure 4.11: Sensitivity of toe penetration in the aquifer central cross section to the freshwater inflow through the inland boundary for different aquifer geometries.

4.4.3 Aquifer Thickness

As stated before, saltwater penetration depends on aquifer thickness provided the remaining parameters are kept constant. Moreover, the effect of the geometry of the aquifer boundaries should be smaller for increasing aquifer thickness, because of the less confinement of the buoyancy term. Therefore, aquifer thickness is one of the parameters that can have the greatest impact on seawater intrusion behavior. In Figure 4.12, the results for different simulations with different values of the aquifer thickness are presented. The higher seawater penetration in the deepest aquifer cross sections for the warped and V-shaped aquifers is still present for all values of aquifer thickness.

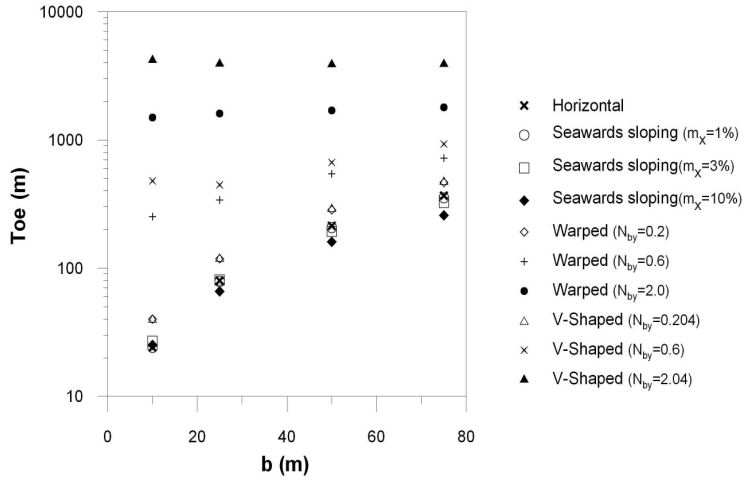

Figure 4.12: Sensitivity of toe penetration in the aquifer central cross section to different aquifer thickness for the different considered aquifer geometries.

4.5 Conclusions

Analysis of seawater intrusion problems is often carried out in vertical cross-sections perpendicular to the sea or areal 2D models using either simplified analytical solutions (based on Ghyben-Herzberg approximation) or sophisticated numerical codes. However, the seawater intrusion patterns in horizontally extensive aquifers are heavily dependent on the shape of their boundaries. Intrusion patterns in aquifers with laterally varying bottom elevation are qualitatively different. The main differences stem from a lateral, essentially horizontal convection cell that develops along the ocean side of the aquifer in aquifers with valley-shaped bottoms. This is due to the slope in the impermeable aquifer bottom in the direction parallel to the coast. Lateral convection cells cause the seawater wedge to penetrate much further inland in the deepest portion of the aquifer.

These effects can be quantified by means of a lateral buoyancy dimensionless number. Lateral convection cells are completely developed with N_{by} numbers higher than approximately 0.4. Modelling such effects requires a full knowledge of the three-dimensional geometry of the bottom aquifer and can only be solved using 3D density-dependent groundwater flow and transport codes. Still, reliable approximations of saltwater penetration can be obtained using the tilted Ghyben-